POLITECNICO DI TORINO

Commission of Environmental and Land Engineering

Master's degree program in
Environmental and Land Engineering

MASTER THESIS

ANALYSIS OF SEISMIC LANDSTREAMER DATA FOR EMBANKMENT INTEGRITY ASSESSMENT

Supervisor:

Dr. Chiara Colombero

Author:

Geraldine Adriana Torres Valero

ANALYSIS OF SEISMIC LANDSTREAMER DATA FOR EMBANKMENT INTEGRITY ASSESSMENT

By

Geraldine Adriana Torres Valero

A thesis submitted in fulfillment of the requirements for the degree of Master in Environmental Engineering.

Department of Land, Environment and Geo-Engineering (DIATI)

Academic year 2020/2021

Graduation session July-2021

Declaration of Authorship

I, Geraldine Adriana Torres Valero, certify that this work titled, "ANALYSIS OF SEISMIC LANDSTREAMER DATA FOR EMBANKMENT INTEGRITY ASSESSMENT" is from my authorship. I also confirm that, from the beginning of this work in November 2020, this thesis was done wholly while in candidature for a degree at this University and it has not been submitted to qualify for any other academic recognition. In addition, all passages that were taken out from consulted published works, were clearly marked as references and the source was always given. Except for such quotations, this thesis is entirely my own work. Finally, I have made clear what was done by others when in some parts of the thesis I needed to work in cooperation with others.

This is the last version of the thesis, containing all the required revisions and accepted by the supervisor.

I am aware of the digital publication of this work.

Geraldine Adriana Torres Valero

Turin, July 15, 2021.

Summary

ANALYSIS OF SEISMIC LANDSTREAMER DATA FOR EMBANKMENT INTEGRITY ASSESSMENT

by Geraldine Adriana TORRES VALERO

Floods, seepages, and animal activities are known to be the main causes of internal damage and erosion of embankments. These factors lead to partial or complete collapse. Embankment integrity losses may progress without any superficial or easy detectable evidence, in consequence visual surveillance or localized techniques are not effective.

Geophysical techniques for characterization of embankments are constantly improving. In literature, there is evidence of numerous advances on the application of electrical and electromagnetic surveys. Refraction and surface wave methods are often less considered because they can be more time consuming. They usually work best to assess vertical velocity profiles of a limited section of the subsurface, without considering lateral variations present in the investigated media, which may lead to erroneous characterization. Nevertheless, in the last two decades, several studies have been published referring to the application of other surface waves methods to assess lateral characterization by detection and location of inhomogeneities in the subsoil.

In this work, four surface wave processing techniques for embankments integrity assessment applied to landstreamer data are tested: energy, energy decay exponent, attenuation coefficient and autospectrum computation. To achieve this objective, classical seismic refraction analyses and the proposed surface wave methodologies were applied and compared. Some limitations related to landstreamer data acquisition were considered during the processing steps: the energy of the source was not constant (manual) for all the common shot gathers (CSGs) and noise was expected to be high. To overcome these limitations, the traces of each CSG were normalized by the maximum amplitude of the trace closest to the source, the stacked results were normalized for the data coverage in order to further balance each shot contribution, and the impact of noise in the quality of results was evaluated. Data interpretation was performed using an empty pipeline within an embankment as a detection target.

Results showed that detection of the pipeline in the velocity model obtained from refraction tomography was precariously accurate and influenced by another geological anomaly located above the target. On the contrary, the proposed surface-wave methodology worked effectively, detecting the pipeline within the embankment. The results of energy and autospectrum depicted high concentrations of energy, centered on the pipeline, but also at surface geological anomalies identified in the velocity model. The energy decay exponent and attenuation coefficient have been shown to be highly sensitive to velocity contrasts

between embankment materials and have shown marked attenuation at both sides of the pipeline. Trace normalization improved the interpretation of the results, and the noise resulting from landstreamer configuration probably had a significant impact on the quality of the negative offset data. The calculation of the horizontal gradient of the four parameters studied allowed to delimitate the position of the pipeline between 28 and 35 m along the reference line studied. From an approximate estimative method based on the wavelengths affected by surface waves, the depth of the pipe is consistent with the real depth.

The combination of these four techniques applied to landstreamer data represents an efficient and rapid tool for monitoring embankments. The effectiveness of these tools was verified for the first time in this work, and it is presented as a novel and fast approach for the assessment of embankment integrity.

Key words: Embankment integrity assessment, energy computation, energy decay exponent, attenuation coefficient autospectrum, SW method analysis.

.

Sommario

ANALISI DI DATI SISMICI ACQUISITI CON LANDSTREAMER PER LA VALUTAZIONE DELL'INTEGRITÀ DI ARGINI

di Geraldine Adriana TORRES VALERO

Inondazioni, infiltrazioni e attività animali sono note per essere le principali cause di danni interni ed erosione degli argini. Tutti questi fattori portano a collassi parziali o completi che possono progredire senza nessuna evidenza superficiale o facilmente rilevabile e, di conseguenza, ispezioni visive o tecniche di indagine localizzate non sono efficaci per il monitoraggio.

Le tecniche geofisiche per la caratterizzazione degli argini sono in costante miglioramento. In letteratura, ci sono prove di numerosi progressi nell'applicazione di indagini elettriche ed elettromagnetiche. I metodi di sismica a rifrazione e analisi delle onde superficiali sono spesso meno considerati perché i tempi di acquisizione ed elaborazione dati possono essere molto lunghi. Generalmente, infatti, questi metodi sono più adatti a valutare i gradienti di velocità verticale di una sezione limitata del sottosuolo, trascurando variazioni laterali nel mezzo indagato, portando a possibili caratterizzazioni erronee. Tuttavia, negli ultimi due decenni, sono stati pubblicati diversi studi relativi all'applicazione di metodi di analisi delle onde superficiali per l'identificazione e la localizzazione di disomogeneità nel sottosuolo.

In questo lavoro, vengono testati quattro parametri estraibili dall'analisi delle onde superficiali per la valutazione dell'integrità degli argini: energia, esponente del decadimento dell'energia, coefficiente di attenuazione e densità spettrale. I metodi sono applicati a dati acquisiti con un landstreamer. Per raggiungere questo obiettivo, sono state applicate e confrontate le classiche analisi di sismica a rifrazione e le metodologie per onde superficiali proposte. Durante le fasi di elaborazione, sono state prese in considerazione alcune limitazioni relative all'acquisizione dei dati con landstreamer. L'energia della sorgente (manuale) non è risultata costante per tutti i punti sorgente acquisiti lungo la linea. Si è inoltre ipotizzato che il rumore fosse elevato a causa della configurazione del landstreamer. Per ovviare a queste limitazioni, le tracce relative ad ogni scoppio sono state normalizzate alla massima ampiezza della traccia più vicina alla sorgente. In seguito, l'insieme dei risultati è stato normalizzato per la copertura dei dati lungo la linea al fine di bilanciare ulteriormente ogni contributo di scoppio. Infine, è stato valutato l'impatto del rumore sulla qualità dei risultati. L'interpretazione dei dati è stata eseguita avendo come obiettivo l'identificazione e la localizzazione di una tubazione vuota all'interno di un argine.

I risultati hanno mostrato che la detezione della tubazione nel modello di velocità ottenuto dalla tomografia a rifrazione è poco accurata e influenzata dall'interferenza con altre anomalie geologiche nelle vicinanze. Al contrario, i metodi per onde superficiali hanno funzionato in

modo efficace, rilevando la tubazione all'interno dell'argine. I risultati di energia e densità spettrale raffigurano alte concentrazioni di energia, centrate sulla condotta, ma anche in corrispondenza di anomalie geologiche superficiali identificate nel modello di velocità. L'esponente del decadimento dell'energia e il coefficiente di attenuazione si sono dimostrati altamente sensibili ai contrasti di velocità tra i materiali dell'argine e hanno mostrato marcata attenuazione ai due estremi della condotta. La normalizzazione delle tracce ha migliorato l'interpretazione dei risultati, e il rumore derivante dalla configurazione di acquisizione ha avuto probabilmente un impatto significativo sulla qualità dei dati con offset negativo. Il calcolo del gradiente orizzontale dei quattro parametri studiati ha permesso di circoscrivere la posizione della tubazione tra 28 e 35 m lungo la linea di riferimento studiata. Da stime approssimate basate sulle lunghezze d'onda interessate dalle onde superficiali, la profondità della tubazione risulta coerente con quella reale.

La combinazione delle quattro tecniche applicate ai dati di landstreamer rappresenta uno strumento efficiente e rapido per il monitoraggio degli argini. L'efficacia di questi strumenti è stata verificata per la prima volta in questo lavoro, ed è presentata come un approccio nuovo e veloce per la valutazione dell'integrità degli argini.

Parole chiave: Valutazione dell'integrità dell'argine, energia, esponente del decadimento dell'energia, coefficiente di attenuazione, densità spettrale, analisi di onde superficiali.

Sumario

ANÁLISIS DE DATOS SISMICOS DE LANDSTREAMER PARA LA EVALUACION DE LA INTEGRIDAD DE LOS TERRAPLENES

por Geraldine Adriana TORRES VALERO

Algunas de las principales causas de daños internos y erosión de los terraplenes son las inundaciones, filtraciones y actividad animal. Todos estos factores generan problemas de inestabilidad que conducen a un colapso parcial o total que pueden progresar sin ninguna evidencia superficial. En consecuencia, el monitoreo visual o técnicas de monitoreo localizadas no son efectivas.

Las técnicas geofísicas para la caracterización de terraplenes han demostrado constantes progresos. En la literatura, hay evidencia de numerosos avances en la aplicación de estudios eléctricos y electromagnéticos. Los métodos de sísmica de refracción y ondas superficiales son muchas veces menos considerados porque los tiempos de adquisición y procesamiento de datos pueden ser muy prolongados y, en general, funcionan mejor para evaluar gradientes verticales de velocidad de una sección limitada del subsuelo, sin considerar las variaciones laterales del medio, lo que puede conducir a una caracterización errónea. Sin embargo, en las últimas dos décadas se han publicado estudios referentes a la aplicación de otros métodos de ondas superficiales para la detección y localización de inhomogeneidades en el subsuelo.

En este trabajo se prueba la efectividad de cuatro parámetros extraíbles del análisis de ondas superficiales para la evaluación de la integridad de los terraplenes: cálculo de energía, exponente de decaimiento de energía, coeficiente de atenuación y densidad espectral. Los métodos se aplican a un set de datos adquiridos por medio de un landstreamer. Para lograr este objetivo, se aplicó y comparó el análisis sísmico de refracción clásico y las metodologías de ondas superficiales propuestas. Durante las fases de procesamiento, se tomaron en cuenta algunas limitaciones relacionadas con la adquisición de datos con landstreamer. La energía de la fuente (placa metálica) no era constante para todos los levantamientos adquiridos a lo largo de la línea. Por otro lado, se esperaban sismogramas muy rumorosos debido a la configuración del landstreamer. Para lidiar con estas limitaciones, las trazas de cada sismograma se normalizaron a la máxima amplitud de la traza más cercana a la fuente. Posteriormente, el conjunto de resultados se normalizo por la cobertura de datos a lo largo de la línea con el fin de equilibrar aún más la contribución de cada sismograma. Por último, se evaluó el impacto del ruido en la calidad de los resultados. La interpretación de los datos se realizó con el objetivo de identificar y localizar una tubería vacía dentro de un terraplén.

Los resultados mostraron que la detección de la tubería en el modelo de velocidad obtenido a partir de la tomografía de refracción es inexacta y está influenciada por la interferencia

con otras anomalías geológicas cercanas. Por el contrario, los métodos de onda superficial funcionaron eficazmente detectando la tubería dentro del terraplén. Los resultados del cálculo de energía y densidad espectral muestran altas concentraciones de energía, centradas sobre la tubería, pero también sobre anomalías geológicas identificadas en el modelo de velocidad. El exponente de decaimiento de energía y el coeficiente de atenuación han demostrado ser altamente sensibles a los contrastes de velocidad entre los materiales del terraplén y han mostrado una marcada atenuación en ambos extremos de la tubería. La normalización de las trazas mejoró la interpretación de los resultados, y el ruido derivado de la configuración del landstreamer probablemente tuvo un impacto significativo en la calidad de los datos con offset negativo. El cálculo del gradiente horizontal de los cuatro parámetros estudiados permitió delimitar la posición de la tubería entre 28 y 35 m a lo largo de la línea de referencia estudiada. A partir de estimaciones aproximadas basadas en las longitudes de onda afectadas por las ondas superficiales, la profundidad de la tubería es consistente con la profundidad real.

La combinación de estas cuatro técnicas aplicadas a los datos de landstreamer representa una herramienta eficiente y rápida para el monitoreo de terraplenes. La efectividad de estas herramientas se verificó por primera vez en este trabajo, y se presenta como un enfoque novedoso y rápido para la evaluación de la integridad de terraplenes.

Palabras clave: Evaluación de la integridad del terraplén, energía, exponente de decaimiento de energía, coeficiente de atenuación, densidad espectral, análisis de ondas superficiales.

To myself…

Acknowledgments

Una famosa oradora dijo que sólo es posible alcanzar la felicidad cuando logras conectar en tu vida con 5 personas claves: un animador, un mentor, un entrenador, un amigo y un colega. En esta ocasión quisiera mencionar y agradecer a mis 5 (y más) personas claves:

La primera y las más importante: mi madre. Gracias por todo lo que me has dado, por tus enseñanzas, por tus amigos, por tu modo de decir y hacer que es mi modo también. Estoy hecha de ti y por ti. Tú eres mi mentor, mi entrenador, mi animadora y mi más grande motivación. Este es mi regalo para ti. Nos vemos pronto.

A mis otros mentores: mi padre, mis queridas hermanas Astrid, Daniela y Andrea, mi adorada tía Cecilia. Ustedes sin quererlo me apuntan siempre en la dirección correcta, que no es necesariamente un lugar si no un modo de ser y reaccionar ante muchas dificultades. Ustedes son mis profesores de vida. Los amo muchísimo.

A mis entrenadores, esos que me sacaron de mi zona de confort para hacerme ver mi potencial en diferentes ámbitos académicos: a mis profesores de la UCV a quienes recuerdo con mucha admiración, y a mis profesores del Politécnico, en especial a mi tutora Chiara Colombero y a mi colega y maestro, Jesús Marval.

A mis amigos de Turín, que conocen mis deseos, que son diferentes a mí y me han permitido abrir la mente y mirar la vida de manera diferente: Rosangela, José Antonio, Scarlet, María José, Giuseppe, Giulio, Estefanía, Luis Alberto, Eimy. A mis amigos de Venezuela dispersos por el mundo, Ali, Carlos, Alejandra. Parte de lo que me convertí es gracias a tenerlos cerca de mí, a pesar de la distancia.

A mi colega, que es también un amigo, pero además está contigo durante tu desarrollo profesional. Dailis, estoy segura de que sin tu empuje y compañía esto hubiese sido menos divertido y más largo. Gracias mi chama.

Además de las "cinco" personas claves, quisiera agradecer también:

A mi familia de El Beso, Tony y Andrea, Potito, Jerry, quienes me acogieron cuando más lo necesité, ¡ustedes son la base de todo lo bueno que pude lograr aquí en Torino y siempre voy a recordarlos como las buenas, humildes y trabajadoras personas que me dieron techo, estabilidad y tequila! Gracias a la vida por ustedes.

A quien considero mi casi todo, Enrico, que en estos meses has sido mi animador y fan número uno, mi amigo, mi mentor y mi entrenador. Te agradezco siempre por tener todo lo que a mí me falta.

A mi segunda casa de estudios en Venezuela, la Universidad Central de Venezuela, por darme tantos momentos de sabiduría y felicidad en sus pasillos y aulas de estudio. Gracias a ti he logrado vencer las sombras, porque sólo un UCVista sabe que la verdadera gloria no es estar sobre las nubes, sino debajo de ellas. Este es mi homenaje para ti.

Y finalmente, quiero hacer un reconocimiento importante al lugar que dejé hace 3 años y que no pensé extrañar tanto cada día. Mi amada y por siempre casa, Venezuela.

Yo soy la suma de todas las veces que me he caído y levantado con éxito, pero para mí el éxito no significa nada si no tengo con quien compartirlo.

Para aquellas personas que han pasado por mi vida para ensenarme algo, y para aquellos que aún lo hacen,

¡Gracias!

Geraldine Adriana Torres Valero.

15/07/2021

Table of Contents

List of Tables

List of Figures

Nomenclature

Acronyms

CSG   Common shot gather.

CPTU   Cone Penetration Test with Piezocone.

ERT   Electrical Resistivity Tomography.

FDEM   Frequency Domain Electromagnetic Induction.

GPR   Ground Penetrating Radar.

IR   Infrared photography.

NED   Normalized Energy Distance Parameter.

MASW   Multichannel Analysis of Surface Wave.

ReMi   Refraction Microtremor.

RMS   Root-mean square.

SASW   Spectral Analysis of Surface Wave.

SCPTU   Cone Penetration Test with Piezocone with measurement of shear wave velocity.

SM   Seismic Methods.

SW   Surface waves.

VSP   Vertical Seismic Profiles.

Notations

γ Energy Decay Exponent.

α_f Attenuation coefficient.

E_i Trace energy at position i.

$G_i(f)$ Autospectral density.

V_p P-wave velocity.

V_s S-wave velocity.

Chapter 1

Introduction

1.1 Foreword

Embankments are susceptible to natural events that can progressively deteriorate the internal and external parts of their structures. The occurrence of floods, seepages and animal activities are known to be the main causes of internal damage and erosion leading to instability problems and degradation of the material properties (Borgatti et al., 2017).

Keeping in mind the above-mentioned issues and considering that river and lake embankments are mainly composed by loose materials, their integrity can be severely compromised with time, as a consequence, partial or total collapse may occur becoming a risk to the surrounding population, reason for which they must be periodically monitored. For this purpose, the most common surveillance practices are mainly based on visual inspection and localized geotechnical measurements, disregarding a whole characterization and possibly leading to erroneous assumptions on their structures (Perri et al., 2014). In order to reduce the uncertainties due to local prospection, specific geophysical techniques

for characterization of embankments are increasing and constantly improving. In the literature, there is evidence of numerous advances on the application of electrical and electromagnetic surveys. Nevertheless, the application of seismic methods for embankments monitoring is limited:

- Di-Prinzio et al., (2010) applied ground penetration radar (GPR) technique to a group of river embankments in the District of Bologna, Italy, focusing on the localization of animal burrows.

- Perri et al., (2014) combined Electrical Resistivity Tomography (ERT), Frequency Domain Electromagnetic Induction (FDEM) and GPR to local embankments of the Tagliamento River in the Province of Venice, Italy. The results were verified through geotechnical techniques (CPTU/SCPTU) finding high resolution similarities between ERT, FDEM and geotechnical methods. GPR results instead, demonstrated not to be reliable at a bigger depth.

- Borgatti et al., (2017) applied a multi-technique approach that combines ERT, FDEM, GPR and infra-red (IR) survey for location of tunnels and burrows.

- Abdulsamad et al., (2019) used induced polarization and self-potential survey for monitoring of leaks over an experimental basin.

- Comina et al., (2020) proposed an alternative configuration of ERT called Electric Streamer, in which electrodes are not attached to the subsoil to make the survey faster. Results were compared with standard ERT methods and showed to be a reliable technique for the acquisition of resistivity data on embankments.

Other traditional techniques, like refraction tomography and surface wave methods, are not considered because they may be more time consuming and work best to assess vertical profiles of a limited section of the subsoil. It has also been demonstrated that the characterization becomes simplified and erroneous if possible lateral variations in the investigated subsurface are not taken into account (Bergamo & Socco, 2014; Boiero & Socco, 2011).

To overcome this limitation, many authors have proposed SW-based computational tools intended to identify lateral discontinuities in 2D sections of the subsurface:

- Nasseri-Moghaddam et al., (2005) developed a SW analysis technique called Attenuation Analysis of Rayleigh Waves (AARW) that computes the energy as a function of the amplitude of each trace in the record. This technique was developed for detection of cavities and their embedment depth.

- Zerwer et al., (2005) computed the autospectral density of seismic traces to detect cracks in concrete structures. Rayleigh waves are strongly reflected in the presence of a crack and this reflection is better represented as a function of the frequency.

- Bergamo & Socco, (2014) applied the autospectrum method developed by Zerwer et al., (2005) and an extension of AARW method to bigger scale synthetic and real data sets. In the AARW extension, energy decay exponent (γ) and the attenuation coefficient (α_f) were applied to multifold seismic data, exploiting data redundancy for the identification of discontinuities.

More recently, Colombero et al., (2019) presented a method which combines the four mentioned techniques: energy, energy decay exponent, attenuation coefficient and autospectrum computation. In this study, the four SW-methods were all optimized for multifold data and tested on 12 2-D synthetic models and 2 field cases. Results showed that all methods can detect and locate lateral inhomogeneities, specifically when these are characterized by acoustic impedance lower than the surrounding material (i.e., fractures, cavities). The combination of these methods was chosen over all the other available techniques because they do not require any data pre-processing, filtering, or muting. They can be directly applied to raw data even during the acquisition; therefore, results can be obtained in a fast way. It was highlighted that the complete application of the four methods, from the uploading of the traces to results requires less than 5 minutes for up to 15 CSGs of 72 receivers.

1.2   Thesis statement

As it was mentioned earlier in the chapter, floods, seepages, and animal activities are known to be the main causes of internal damage and erosion of embankments, all of these factors generate instability problems and degradation of the material properties ultimately leading to partial or complete collapse. Embankment integrity losses may progress without any physical, superficial, or easy detectable evidence, in consequence visual surveillance or localized techniques are not quite effective.

The present work proposes the application of the four methods applied by Colombero et al., (2019): computation of energy, energy decay exponent, attenuation coefficient and autospectrum to a seismic data set recovered by a landstreamer. The application of these combined SW analyses is presented as a novel, effective and alternative tool for monitoring embankments. It takes advantage of its potential for locating lateral variations due to the direction of propagation of SW, parallel to the ground surface, and fast applicability, since no pre-processing of the data or a previous geological knowledge on the embankment structure is needed.

A field case study of landstreamer data acquired on an embankment will be used to evaluate the effectiveness and advantages of the proposed methodology. To do so, two different approaches will be followed and compared: first, the use of traditional refraction tomography to generate a velocity model along the investigated embankment. Second, the implementation of the four SW-methods proposed by Colombero et al., (2019) for landstreamer data. The interpretation will be performed focusing on the location of the pipeline within the embankment.

Results from SW-methods will be interpreted highlighting their advantages with respect to the velocity model obtained through refraction tomography, which is considered in this work as a traditional seismic tool.

1.3   Motivation and objectives

The use of the four SW-methods applied to landstreamer data is presented in this work as an innovative and alternative tool for embankment integrity assessment. Since monitoring must be an imperative task, the importance of the proposed methodology relies on faster intervention after the identification and location of potential hazards.

Within the motivations, it is emphasized the novelty of the method, that combines a fast data acquisition, using a landstreamer system, with an effective processing tool suitable for real time screening, exploiting many important features of SWs (horizontal propagation, less attenuation and highest amplitude). Besides, this work aims to bridge the knowledge gap regarding to the use of SW-methods for embankments monitoring.

The principal objective of this work is to evaluate the effectiveness of processing landstreamer seismic data through four SW-methods: Energy, Energy Decay Exponent, Attenuation Coefficient and Autospectrum.

1.4   Limitations

Some limitations concerning the acquisition of the data will be considered in the processing steps. First, a hammer was used as manual source for all the shots. Consequently, the source energy was not constant for every CSG. Since in a landstreamer acquisition the receiver positions are generally only partially overlapping between subsequent shots, this could lead to unbalanced computations along the investigated line and eventual misinterpretations. Second, due to the configuration of the landstreamer, geophones where not attached to the ground, therefore the noise in the CSG is expected to be high. For the last, the path of the landstreamer was not setup to cover the subsoil in a homogeneous way.

To diminish these constraints, it has been proposed to:

1. Normalize the traces of every CSG by the maximum amplitude of their first trace (i.e., the closest to the source), obtaining a uniform shot contribution along the total profile.

2. Evaluate whether the noise due to the acquisition setup is an important matter in the quality of the results and can be practically avoided in future acquisitions.

3. Normalize the results at each receiver locations by the number of times at which this position was sampled. This sampling concept for each position along the line will be further referred to as "coverage".

4. Compute the horizontal gradients of the stacked results of each method as quantitative location criteria.

5. Provide a rough indication of the embedment depth of the target.

1.5   Case study

The site of interest is located on the south shore of the Arignano Lake, in the municipality of Arignano (Turin). This was originally a depressed area with a vegetal cover that needed to be delimitated downstream with a barrage/embankment to enclose the lake, as shown in Figure 1.

Figure 1. Plan view of Arignano lake. Extracted from Google Maps.

The embankment was constructed with loose material in 1830 and the lake served as a reservoir to the nearest fields. In 1980 was completely drained and refilled in 2005 (PiemonteParchi, n.d.).

The dimensions of the embankment are approximately 7 m high (Fazio, 2019) and 345 m long and it has a flat crown of about 5 m width. The presence of a pipeline, that was used to provide water from the reservoir to mills located downstream, is depicted at approximately 45 m from its eastern edge (Figure 1). The diameter of the pipeline is 2,8 m. It is buried at 2

to 4 m deep and surrounded by a concrete structure of length 6,5 m which comes out to the surface from the crown of the embankment (Figure 2). Nowadays, water supply is no longer active, consequently the pipeline is empty.

In the interpretation phase, significant anomalies are expected to be found in the seismic parameters because of the contrast between the loose material of the embankment and the concrete structure containing the pipeline or the air/water content inside. This contrast makes this localized buried object an excellent target for testing the effectiveness of SW-methods for the detection of lateral inhomogeneities within the embankment.

Figure 2. Picture of the embankment and the concrete structure enclosing the pipeline. Extracted from PiemonteParchi, (n.d.).

1.6   Electrical methods used at the Arignano Lake

Electrical methods consist in the analysis of the effects produced in the ground after the injection of an electrical current flow, knowing that every material has a different response to that current. The retrieved parameter is the electrical resistivity of the surveyed materials. This physical quantity varies significantly in presence of water, making electrical methods highly effective for detecting water reservoirs. The depth of prospection that can be reached depends on the length of the survey line and the configuration used to inject the current.

In this work, an electrical survey acquired on the Arignano Lake embankment (Comina et al., 2020) was considered as complementary characterization tool. For the acquisition, an electrical streamer, with electrodes located at 1-m distance, was used. The total length of the line was 140 m, resulting in an investigation depth of approximately 26 m. The ERT results (Figure 3) clearly depicted the presence of the pipeline structure. The model has a range of electrical resistivity ranging from 15 to 29 Ωm. These low-resistivity values are typical for the silty clay impermeable materials constituting the embankment. Overall, the electrical resistivity is decreasing with depth. The most significant anomaly, that is related to the location of the pipeline structure is depicted in the model between 80 and 96 m from the reference point, the anomaly has a resistivity of > 29 Ωm and is approximately 10 m long

and 10 m deep. The size of the electrical anomaly is however highly overestimating the real size of the pipeline and surrounding structure, probably due to the resolution of the method. Surface wave methods will be tested in comparison to see if the target is better identified in the seismic results and its location can be improved.
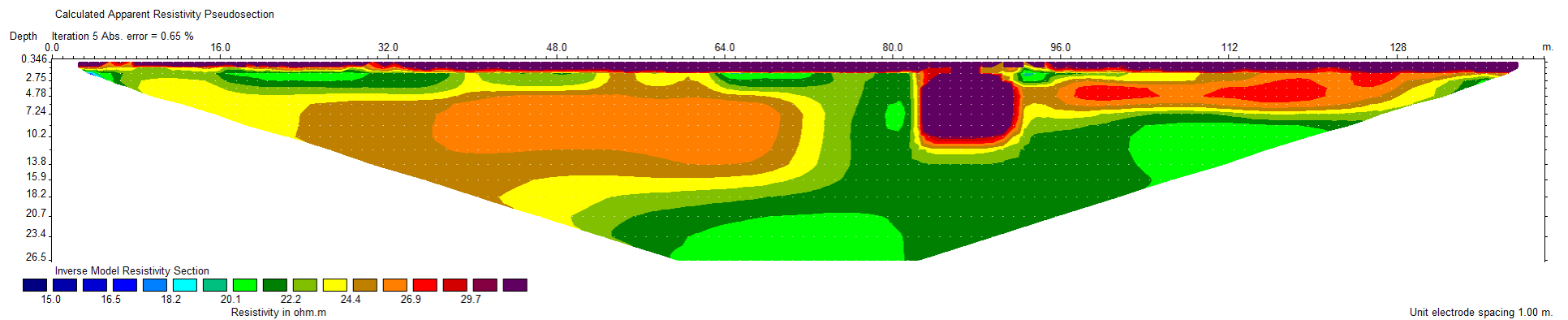
Figure 3. Electrical resistivity tomography. Extracted from Comina et al., (2020).

1.7 Thesis structure

This thesis consists of five chapters structured and detailed as follows:

Chapter 1 represents the foreword of this work. It starts with a brief introduction to provide the reader with insights into this thesis work, presents the thesis statement, motivation, objectives, and limitations. Finally, the case study and some literature studies are also presented.

Chapter 2 presents the theoretical framework. It introduces the reader into the field of seismics, from the definition of waves to the computational tools used to achieve the objective of this work.

Chapter 3 describes the methodology of the traditional (reflection tomography) and innovative (SW tools) seismic data processing. Details of the tomographic procedure and input parameters for the generation of the velocity model using GeoTomCG are presented. The chapter continues with a description and input parameters of every MATLAB code used to develop the four SW-methods: computation of Energy, Energy Decay Exponent, Attenuation Coefficient and Autospectrum.

Chapter 4 presents the results obtained from each seismic method. It begins with the considerations made to obtain the final version of the velocity model and the related qualitative interpretation. Subsequently, results obtained by the four SW-methods are presented, for both positive and the negative offsets. The last section of the chapter presents the joint interpretation of the stacked positive-negative offset results.

Chapter 5 summarizes the conclusions of this work in accordance with the established objectives. Finally, recommendations for future works are given.

The complete workflow and thesis structure is presented in Figure 4.
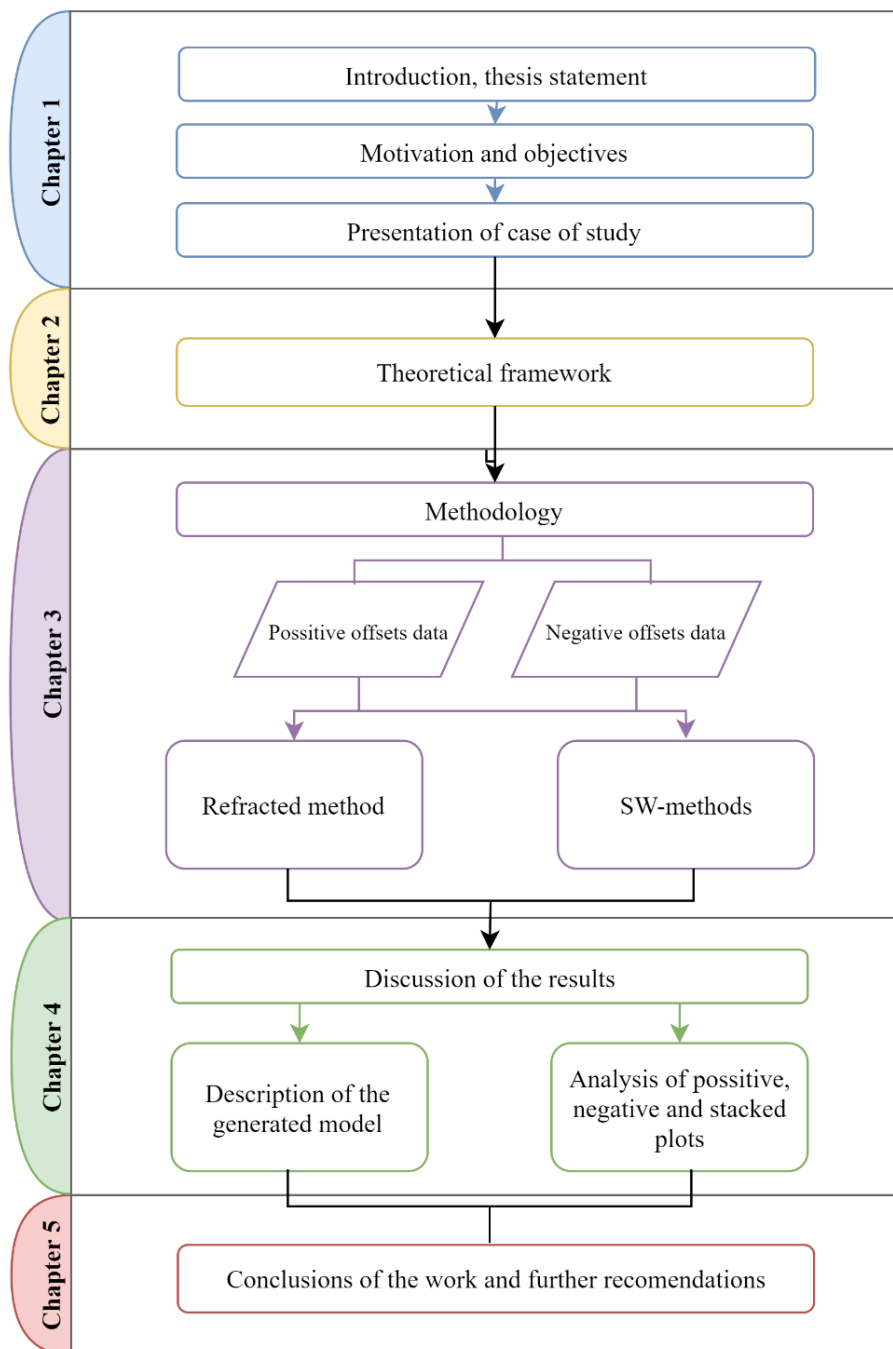
Figure 4. Thesis structure workflow.

Chapter 2

Theoretical Framework

2.1 Properties of waves

A wave can be defined as a disturbance that carries energy from one point to another. Seismic waves are elastic waves, meaning that deformations in the media caused by them are not permanent, so the medium returns to its original state once the energy has been passed into a next part of the medium. The response of waves particles traveling through a material comes from repeated compressional and tensional motion. The propagation is given by the wave equation and their velocity depends on the properties of the media such as porosity, presence of water, compaction, temperature, and pressure (Gonzalez, 2011).

Waves that travel through a medium experience different types of motions that can be describe through:

- Huygens 'Principle: every point on a wavefront can be regarded as a new source of waves and every wavefront generated interfere mutually (Telford et al., 1990).

-   Snell's Law or Refraction Law. When a wave finds another medium with different acoustic impedance, part of the energy is reflected with a certain angle θ_1 and remains in the same medium with its velocity V_1. The rest of the energy is refracted with a different angle θ_2 into the other medium that has different velocity V_2 (Telford et al., 1990):

$$\frac{\sin \theta_1}{V_1} = \frac{\sin \theta_2}{V_2} \qquad (1)$$

-   Diffraction phenomenon involves a change in direction of waves as they pass through an opening or around a barrier in their path. The amount of diffraction increases with increasing wavelength. As a matter of fact, when the wavelength of the waves is smaller than the obstacle, no noticeable diffraction occurs (Telford et al., 1990).

-   Dispersion is related to differences in phase velocities *V* that are inside a portion of the signal that travels with another velocity. This portion is known as group velocities *U*. If *V* do not change with frequency, then *V* and *U* will be equal and there will be no dispersion. When *V* changes with frequency, as for surface waves, *V* is different from *U* and the medium is known as dispersive. In literature, there is evidence that dispersion expected for body waves is small. On the contrary, this phenomenon is strongly connected with surface waves because they experiment high velocity variations with frequency (Sheriff & Geldart, 1995).

2.2 Seismic waves

Seismic waves that propagate in solids and fluids are characterized by their different propagation direction. Every existing analysis is dependent on the type of wave studied and its trajectory through the media. Based on this, two types of seismic waves are known: body waves (BW), that propagate in all directions, and surface waves (SW) that propagate mostly shallow and parallel to the ground surface (Lange & Schuck, 2007).

2.2.1.   Body waves

Body waves travel in the interior of a medium, faster than surface waves. Based on the arriving order to reach the recording unit, body waves are classified in primary (P-waves) and secondary waves (S-waves):

-   Primary waves (P-waves) are also known as compressional, irrotational or longitudinal waves. Because of their high velocity of propagation, they arrive first to geophones. They oscillate in the direction of the propagation of the wave; according to the trajectory through the media they can be classified in direct, reflected,

refracted, with critical angle and front waves. Direct and refracted waves are mostly used in refraction analysis.

- Secondary waves (S-waves) also called shear waves or shaking waves, travel with a lower velocity than primary waves and are detected secondly by geophones. They are transverse waves because they oscillate in the vertical and horizontal plane, perpendicular to the direction of propagation, giving to S waves the property of having two modes: S_h and S_v (Sheriff & Geldart, 1995). S-waves cannot propagate in fluids because fluids do not support shear stress.

2.2.2.   Surface waves

They are named surface waves because their amplitude decreases exponentially with increasing depth, they travel only near the surface which represents the boundary of a non-infinite nor homogeneous medium (Telford et al., 1990). Surface waves or boundary waves, are generated in all types of seismic surveys and are usually characterized by their low velocity and large amplitude, besides, they have the strongest energy and can be described as dispersive waves, which means they have different wavelengths traveling with different phase velocities, and this velocity depends on the frequency (Park et al., 2007).

Different types of surface waves are known:

- Rayleigh waves (also called ground roll) are a combination of longitudinal and transverse motions in a vertical plane that includes the direction of propagation. These motions are described as elliptical and retrograde because they are opposite to the direction of motion of the particles in waves on the surface of the water. The amplitude decreases exponentially with increasing depth. They travel slower than shear waves because of the elastic constant of the material (Telford et al., 1990).

- Love waves are shear waves that oscillate only in the horizontal plane through a superficial media with a lower velocity than in the subjacent layers. They travel slower than P and S waves, but faster than Rayleigh waves (Dobrin, 1960).

2.3 Seismic methods

Seismic methods (SMs) are a significant area of the geophysics based on the study of elastic waves propagation inside the Earth. The basic principle of all seismic methods is the analysis of elastic waves either naturally occurring or artificially generated in order to image the subsurface. Because of their high accuracy, resolution, and good penetration, SMs are not only used frequently during exploration and characterization of petroleum reservoirs, but also for civil and environmental engineering tasks (Telford et al., 1990). These methods are implemented in three progressive steps: starting from the seismic data acquisition campaign,

the raw data are then processed for a better visualization and representation and finally, the interpretation phase is performed to associate the seismic model to the background geological or engineering model. The final result is the estimation of important mechanical properties of a volume of the media in which waves are travelling.

The most important parameter in seismic methods is the velocity of propagation of seismic waves. Velocity depends on the properties of the media such as bulk density as well as elastic properties and it varies with mineral content, lithology, porosity, pore fluid saturation and degree of compaction (Lange & Schuck, 2007).

Each type of seismic survey uses a specific type of wave (for example, refracted waves for refraction survey) and its specific arrival pattern on a multichannel record. According to the trajectory of the waves through the subsoil, seismic methods can be principally classified as follows:

- Reflection method: uses P- or S- waves that are reflected at geological boundaries characterized by density and velocity contrasts and travel back to the surface. They are used mostly in the petroleum and mining industry for exploration and characterization of large and deep volumes of material. Depths that can be reached using this method are about several km.

- Refraction method: usually exploits P-waves. It is based in the Snell's Law that describes the trajectory of refracted waves through a media. This seismic method requires that the acoustic impedance of materials increases with depth. The maximum depth reached is about 1/3 of the total length of the survey line. It is the most used technique within civil engineering for characterization of shallow layers, down to 10-30 m depth.

- Surface waves methods: usually exploit the dispersion of Rayleigh waves in the frequency domain to estimate variations in the velocity of propagation of S-waves with depth. Its application is mainly aimed to obtain geotechnical information of the subsoil.

- Specialized techniques such as Vertical Seismic Profiles (VSP) and Crosshole Tomography. VSP exploits P and S-waves travelling from the source located at surface and a geophone located at a certain depth within a borehole. On the contrary, Seismic Crosshole Tomography considers the trajectory of direct waves travelling along paths between two points located at the same depth but in two different boreholes. Both methods are used mainly to obtain the dynamic elastic modulus of the subsoil for geotechnical purposes.

2.3.1.   Acquisition of the data

A data acquisition system is essentially constituted by a seismic source, seismic receivers (geophones) and a recording unit (seismograph). During the acquisition process, a source is used to generate seismic waves that are transmitted to the Earth. The response or the returning waves are recorded by the geophones positioned on the surface in a pre-establish geometry at different offsets or incremental distances away from the source. For the last, signals are transmitted along seismic wires from the geophones to the recording unit.

In the acquisition campaign, seismic waves are generated by artificial sources such as explosions and vibrating machines or by natural earthquakes happening in the Earth's crust. Some of the artificial impacting machines are:

- Hammer: is the most basic tool and consists of a metal plate positioned in the ground at a known distance from the first geophone and a hammer used by an operator which strikes the plate. This type of source is commonly used in refraction methods.

- Explosives: commonly used in a big scale surveys where is necessary to reach major depths. The resolution of this type of source is very good because of the high volume of energy released to the ground.

- Thumper truck: is a sophisticated type of source that is composed by a truck unit with a ground impact system. This impact system carries a heavy weight that is repeatedly dropped from the back of the truck.

Geophones are located at a known distance from each other and from the source and are positioned along straight profile lines (2D seismic) or over an area in 3D seismic surveying. The distance between the source and first receiver determines the largest wavelength developed in the measurements (near field effects), and the distance between geophones determines the smallest wavelength obtainable from the data that works as a resolution indicator (Miller & Steeples, 1994)

2.3.1.1.   Landstreamer acquisition

Some other configurations may be used for data acquisition. A landstreamer is an array of geophones designed to be towed with a mobile unit along the ground, see Figure 5. It is composed by the traditional equipment used for seismic acquisition: source, seismic receivers and a recording unit, the main difference is that geophones are not inserted into the ground during the acquisition. This setup enables for faster acquisitions, but reduced the coupling between receivers and the ground, potentially introducing noise in the recorded data.
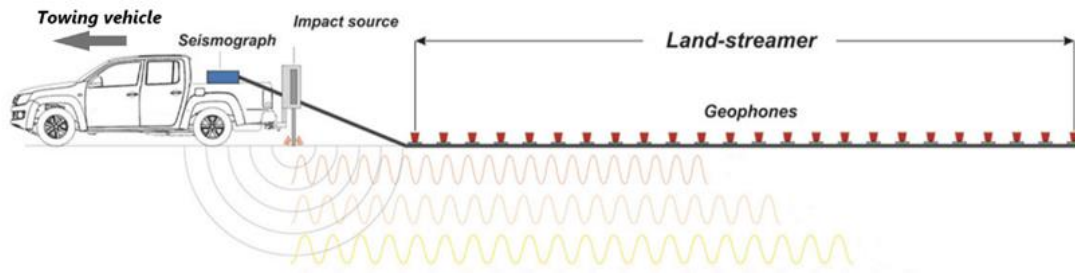
Figure 5. Representation of all the parts of a landstreamer system. Extracted and modified from Everest Geophysics S.L.,(2020).

For this reason, geophones have an added weight at the bottom to ensure their contact with the soil, without affecting the efficiency of the acquisition (LLC n.d.). Woven belts or steel wire ropes are also employed to keep the distance between geophones. Once the path has been predefined, the mobile unit stops for a few seconds and the mechanical source beats the ground generating high-amplitude surface waves. This system results in a faster acquisition method and thereby acquisition costs are reduced. Landstreamer technology has gained an increase in interest and use for the past 15 years. First landstreamers were constructed and tested by Van Der Veen & Green, (1998) and Van der Veen et al., (2001) their main interest was focus on rapid P-wave seismic reflection acquisition. More recently, new landstreamer designs have been developed and used with shear wave source and receivers (Liberty & Gribler, 2014).

No matter what type of the array for the acquisition is used, the result of the acquisition is a file with the recorded time in seconds and a series of curves containing the response of every type of wave traveling in the subsoil, in terms of amplitude and frequency. These curves are called traces and its graphic representation is called seismogram. When more than one geophone is recording the signal coming from the same source, the seismogram is also called Common Shot Gather (CSG) and contains the amplitudes of every wave arriving to each geophone located a different distance from the source.

2.3.2.   Data processing and interpretation

Once the acquisition campaign is completed, the processing of the data requires computational tools to generate a clear representation of the data for its later interpretation. When a seismic survey is performed, all types of waves are generated, however for the processing, only one type is considered as "signal", while the others are usually considered as "noise" and are thus filtrated in order to improve the signal-to-noise ratio. Most existing methods achieve the characterization of the subsoil by processing the signal in time or frequency domain, to estimate the velocity of propagation of waves in the subsoil. The velocity of propagation is affected by the composition of each layer and its related to physical and mechanical properties (i.e., density, compaction, elastic moduli, water content).

Generally, processing strategies are affected by acquisition parameters and shallow soil conditions, such as hydrographic and demographic restrictions (presence of a river or urban areas). These restrictions have a significant impact on the quality of the acquisition, and in consequence, in the quality of the results. To ensure better results during processing, acquisition campaigns are organized to guarantee redundancy of data, which means an improvement of the signal in terms of coverage, or number of traces for common points (Manzoni, 2001). In some other cases, improvement of seismic signals can only be performed with processing techniques.

Processing techniques will depend on the type of analysis, from geometric spreading corrections, application of Fourier transforms or f-k filtering, to sophisticated methods to modify the trace amplitudes using gain functions g(t) in the time domain. Other applications such as deconvolution, stacking and migration of the signal are common within reflection analysis (Yilmaz, 2000). The final result is a 2D-3D model with a reliable representation of vertical variations of the velocity and even thickness of each layer. The interpretation of such models becomes more effective with the knowledge of a geological background (Telford et al., 1990).

2.4   Refraction methods

This method considers body waves with paths that follow Snell's Law, meaning that after the generation of the seismic waves, part of the energy is refracted and travels within the limit of two layers, with the velocity of the deepest one, to finally return to the surface with the velocity of the first media, as shown in Figure 6. Refraction method can be applied only when velocity increases with depth, layers with insufficient contrast in acoustic impedance or thickness cannot be detected by the method (Ibrahim, 2015). Refraction method shows better results when the layers present high contrasts in acoustic impedance (Z= ρV, Gonzalez, 2011).
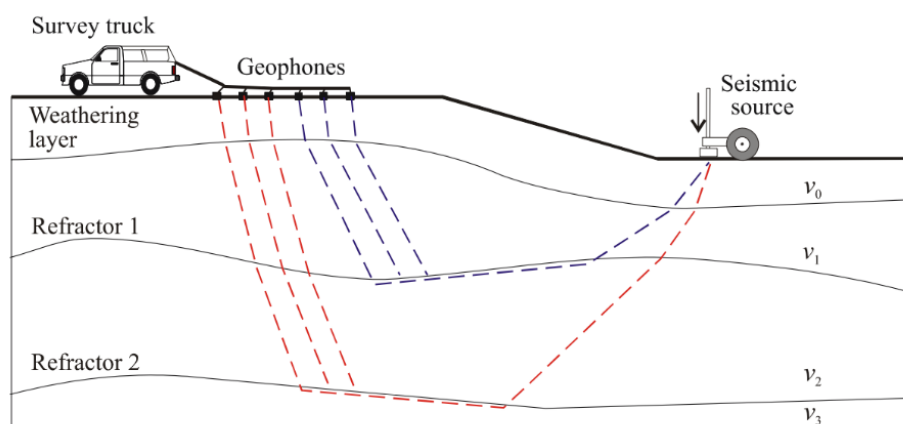

Figure 6. Refracted ray paths propagation. Extracted and modified from Lange & Schuck, (2007)

In refraction analysis, surface waves are usually considered as noise, therefore they are eliminated or reduced to improve the signal quality. A cautiously method of selection of first arrival time, meaning the selection of P-waves times, is needed. Inversion methods are used to fit the experimental observations with a velocity model that adjust the most to a geological background, consuming a considerable amount of time to obtain a reliable result.

Refraction surveys are commonly used for shallow prospection within the geotechnical field where the stiffness of the subsoil and the location of bedrock surface are needed (Fitts, 2013).

Advantages:

- Data acquisition is less time consuming than reflection seismic and direct methods.
- It is a cost-effective method since no perforation is needed to set the equipment.
- Complex machinery is not required.
- It is an easy and fast method.
- The obtained data reflects approximated features of a volume of soil, not punctual values.

Disadvantages:

- Low resolution, the method cannot differentiate thin or very similar strata.
- It does not provide univocal lithological information.
- The highest depth that can be reached is proportional to the length of the survey line.
- Resolution decreases with depth.
- The use of explosives can increase the quality in the registration, but perforations are needed, so the cost of employing the method increases as well.
- Refraction methods are not functional in homogeneous or structural complex media, nor in igneous and metamorphic rocks and zones with high attenuation of seismic waves.

2.5   Surface wave methods

In surface wave methods, even though surface waves are commonly considered as noise, they contribute with significant information about material properties of the shallow ground. All signals considered as noise are generally filtrated from the seismogram in the refracted methods, i.e., Rayleigh waves, but are the main focus in surface waves analysis. R-waves

are generated and recorded easily, the large amount of energy they carry is close to the surface, and they are less attenuated than body waves with distance (Miller & Pursey, 1954).

Surface wave methods are mostly used for vertical characterization of the ground by determination of shear waves velocities, V_s (Bergamo & Socco, 2014). This V_s is linked to the stiffness of the material, which is an important geotechnical parameter.

These methods can be performed in an active form (using artificial mechanical sources) like Spectral Analysis of Surface Waves (SASW) and Multichannel Analysis of Surface Waves (MASW). There are also performed in a passive form that uses natural sources like ambient noise (thunder and tidal motion, traffic in urban areas). They all have the same theoretical basis which consist in a spectral analysis to retrieve the dispersion of Rayleigh waves (Gonzalez, 2011). Differences between methods rely on the target and depth of penetration, that varies with the wavelength.

<u>Advantages:</u>

- They are not invasive methods, thus is not necessary to drill holes for explosives or potentially dangerous sources.

- There is no damage or need of structure conditioning before using these methods.

- Contrary to the refracted methods, these methods can be used in any horizontal stratigraphic context. There are no limitations of velocity inversions associated to low-velocity strata between compact layers with higher velocity.

- There are easy and fast execution methods.

<u>Disadvantages:</u>

- They are unable to reach major depths, except in hard rock sites.

- Processing of the experimental data can be quite complex.

- Misinterpretation of fundamental mode in the propagation of SW, that leads to wrong estimation of velocities.

- Media with strong lateral variations cannot be modelled with standard 1D SW analysis.

2.6 Surface wave methods for identification of lateral variations

Surface wave methods mentioned in the previous section are intended to generate subsurface velocity models using specialized computational programs to assess only vertical gradients. Taking this into account, the location and the representation of inhomogeneity shapes along the horizontal profile are not the main objectives (Bergamo & Socco, 2014). Minor 2D or 3D lateral variations can be modelled using standard strategies as in an equivalent 1D medium, on the contrary, if sharp 2D or 3D inhomogeneities are present, the equation for horizontal layers cannot be used (Foti et al., 2018). Not considering lateral variation may lead to generate erroneous velocity models. In the literature, several techniques are proposed to solve this limitation.

In the next section some of these methods to identify and locate lateral variations based on SWs will be presented, through computational tools that exploit SW trajectory parallel to the ground and the high energy that remains longer in the recordings. This approach results in different ways to process the signal and to obtain many visual representations of the signal energy to detect and locate the presence of faults, intrusions, and cavities.

2.6.1 Energy, E_i

This technique was developed by Nasseri-Moghaddam et al., (2005) as the first step of the Attenuation Analysis of Rayleigh Waves (AARW) for detection of cavities and their embedment depth.

This method is based on the computation of the energy E_i contained in each trace of the CSG as the sum of the square spectral amplitudes $A_{f,i}$, followed by a correction to recover geometrical spreading, by multiplying each value of energy for the distance r_i of the geophone from the source:

$$E_i = \sum_f |A_{f,i}|^2 r_i \tag{2}$$

The next step is to normalized all energy values by the maximum value in the CSG, obtaining the *Normalized Energy Distance Parameter* (NED) which is a dimensionless parameter with values between 0 and 1 (Nasseri-Moghaddam et al., 2005):

$$NED_i = \frac{E_i}{max(E_i)} \tag{3}$$

The final results are *E-r* plots where discontinuities are expected to be visually represented as fluctuations of the energy.

- Nasseri-Moghaddam et al., (2005) applied the method to different model configurations of homogeneous materials containing a void. Some of the conclusions were that the material becomes dispersive, and the wave front is attenuated because of the reflection and diffraction generated by the void. For every model configuration tested, in *E-r* plots the void is clearly represented by peaks of energy at the beginning of the void and sharp decays after it. *E-r* plots for four different cases are shown in Figure 7, the arrows indicate the position of the boundaries of the cavities.
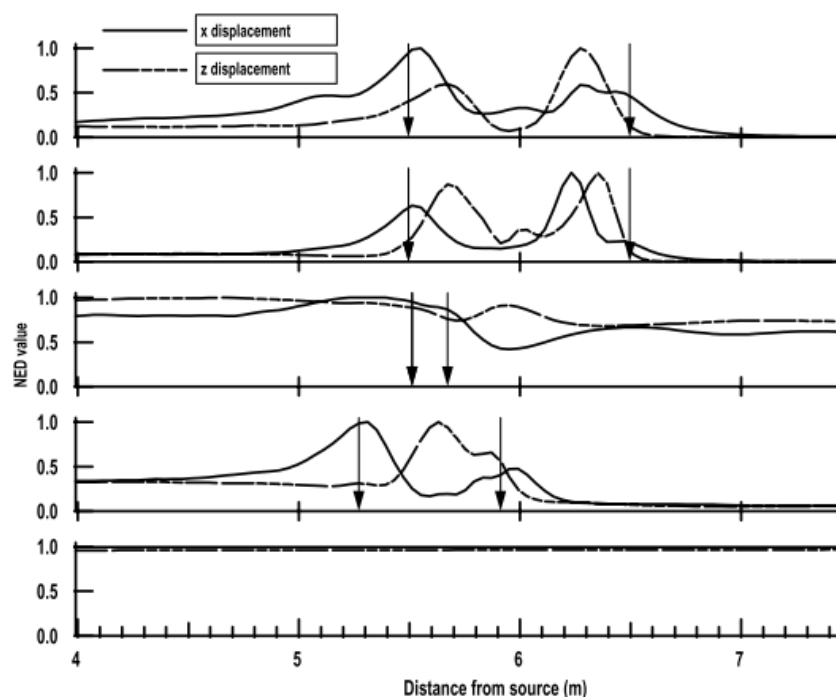

Figure 7. Variation of NED parameter with distance for four different cases. Extracted and modified from Nasseri-Moghaddam et al., (2005).

- Bergamo & Socco, (2014) applied this technique to both synthetic and field cases for detection of lateral discontinuities in combination with other methods. Their results were consistent with those obtained by Nasseri-Moghaddam et al., (2005), thus finding an energy concentration in the proximity of the discontinuity and sharp decays just after it.

- Colombero et al., (2019) evaluated the application of the method to multifold data by stacking and renormalizing *E-r* plots obtained from every CSG. This renormalization is performed to reduce the influence of the source in every single shot and allows a good visual representation of anomalies. The authors describe many scenarios where energy peaks are present within discontinuities with lower

velocity that the surrounded medium (Figure 8.a), and a contrary response for the opposite configurations (Figure 8b).
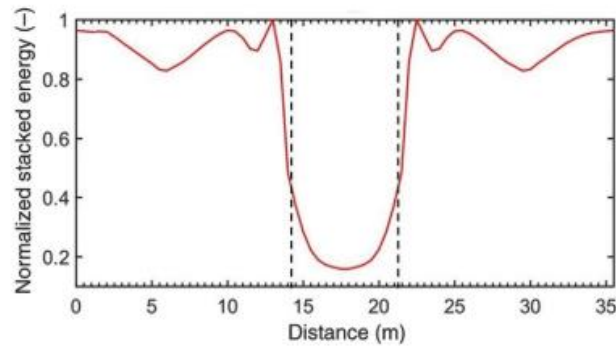
a)
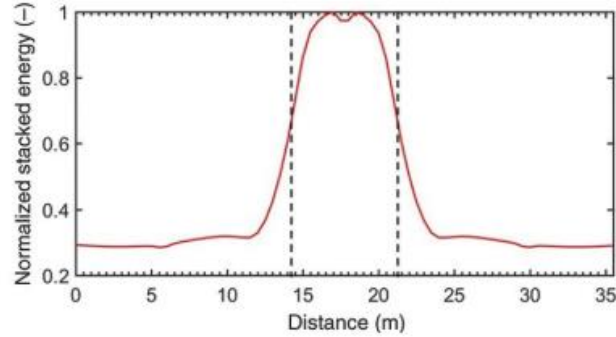
b)

Figure 8. Normalized stacked Energy plot for two different configurations. a) low-velocity and b) high-velocity body located within the dashed lines Extracted and modified from Colombero et al., (2019).

2.6.2 Energy decay exponent, γ

This method was developed by Bergamo & Socco, (2014) by adapting the AARW method to multifold seismic data as a way to take advantage of their redundancy, to increase the reliability and estimate uncertainties through the energy decay exponent γ. The method is applied by considering the values of energy and distance within a window that shifts along the *E-r* plot obtained for every CSG in the first method, where γ is the slope of every portion of the window considered in bilogarithmic scale:

$$log \left(\frac{E_{i+1}}{E_i}\right) = -\gamma \ log \left(\frac{r_{i+1}}{r_i}\right) \qquad (4)$$

The result is an average value of γ computed on each window from all CSGs. In a homogeneous medium, the value of γ is expected to be zero if geometrical spreading is recovered. Values different from zero are responding to the reflection of the waves onto the lateral variations and are depicted as energy decays or concentration of energy when $\gamma > 0$ and $\gamma < 0$ respectively. In acquisitions with available positive and negative offset

recordings (i.e. shots located on both left and right sides of the receivers), the trends in the $\gamma - r$ plots are expected to be opposite at the location of the discontinuity because of the interaction of the incident and reflected waves at the interface (Colombero et al., 2019).

- Bergamo & Socco, (2014) applied this method to multifold synthetic and field data and found that the adapted AARW method can effectively represent the behavior of energy propagation in the presence of near-vertical discontinuities. They proved in the field data application that strong lateral variations can be visually located in zones of the $\gamma - r$ plots where the trend of positive offsets values change from low to high values and negative offsets have the opposite response as shown in Figure 9. The dashed lines represent the exact location of discontinuities.
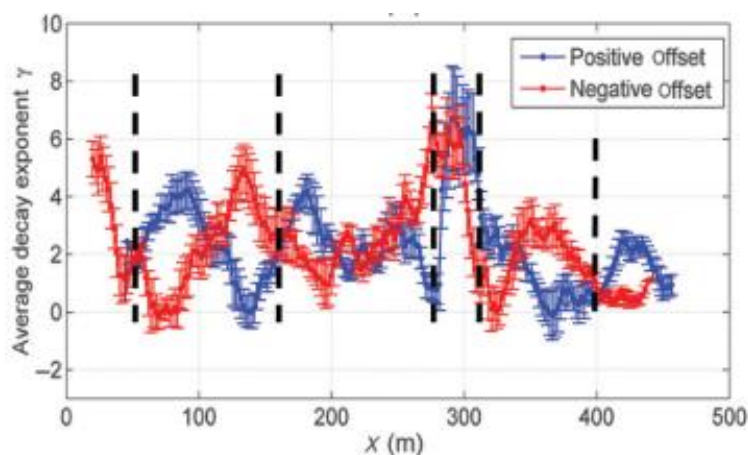

Figure 9. Response in terms of $\gamma - r$ of a fault system. Extracted and modified from Bergamo & Socco, (2014).

- Colombero et al., (2019) applied the method to synthetic and field data. The authors suggested to plot $-\gamma$ results since, for synthetic models, energy concentration was noticed when discontinuities have lower velocity than the medium that surround it (positive peak). On the contrary, energy decays (negative peaks) were noticed when the contrast between the materials was opposite. They also demonstrated that higher contrasts in the acoustic impedance of the materials increase the amplitude of the peaks. The location of the discontinuities can be successfully correlated between positive and negative offsets (Figure 10). Results for the field data confirmed the expected behavior.
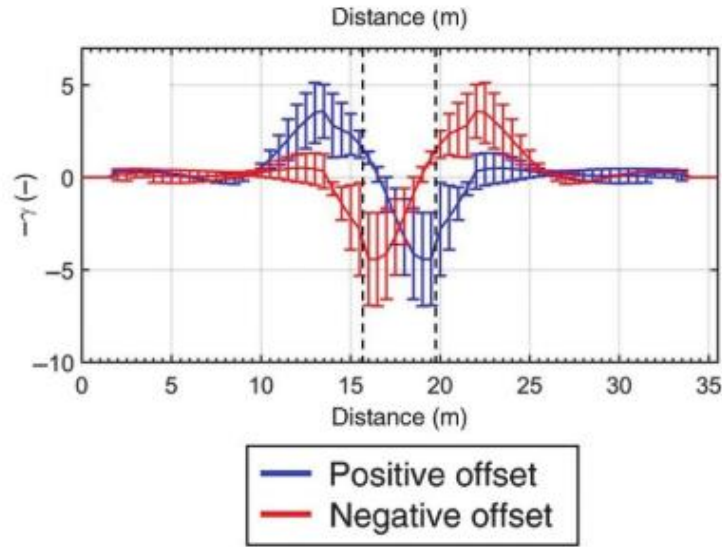
Figure 10. Energy decay exponent results on a low-velocity heterogeneity with edges located at dashed lines. Extracted and modified from Colombero et al., (2019)

2.6.3 Attenuation coefficient, α_f

This parameter is also considered in the adapted AARW method proposed by Bergamo & Socco, (2014) and allows to detect lateral variations by measuring the value of local attenuation of the propagating wavefield at different frequencies. The computation starts from the equation describing the energy decay of Rayleigh waves due to intrinsic attenuation for frequency component and after compensating for geometrical spreading:

$$ln\left(\frac{E_{f,i+1}}{E_{f,i}}\right) = -2 \propto_f (r_{i+1} - r_i) \tag{5}$$

As for the energy decay exponent calculation, the attenuation coefficient is the slope of the *E-r* plot (with *E* in natural logarithmic scale) of a portion within a moving window that moves along the traces. For each frequency contribution, the attenuation coefficient is computed as the relation of the values of energy in natural logarithmic scale at two subsequent geophones in the positions *i* and *i+1* with distance from the source r_i and r_{i+1}. Lateral variations are represented as a function of the value of $\propto_f$, and values are normalized to equalize the frequency contribution along the line by:

$$\overline{\Delta\alpha_{f,w}} = \frac{\overline{\alpha_{f,w}} - \overline{\alpha_{f,}}}{stdev\left(\overline{\alpha_{f,}}\right)} \tag{6}$$

Attenuation coefficient is related to mechanical properties of the subsoil that are influenced by the propagation of SWs in different frequency components. When strong variations of α_f are found, it is the consequence of the back reflection and attenuation of the energy at the interface (Xia et al., 2002).

- Bergamo & Socco, (2014) applied this method to multifold synthetic and field data and found that even if the attenuation coefficient analysis appears lees comprehensible that energy decay exponent, it allows to distinguish the frequency band whose propagation is affected by discontinuities. They highlighted the importance of the separate analysis of positive and negative offsets because it allows to evaluate opposite behavior between both results.

- Colombero et al., (2019) introduced another way to represent the results by stacking the absolute values of positive and negative values of $\overline{\Delta\alpha_{f,w}}$ and plotting the stacked results $\overline{\Delta\alpha_{STACK}}$ as a function of the distance, where:

$$\overline{\Delta\alpha_{STACK}} = \overline{|\Delta\alpha_{POS}|} + \overline{|\Delta\alpha_{NEG}|} \tag{7}$$

For the synthetic models, stacked plots are showing improved results and allow for a clear delineation of the targets (Figure 11). There is an energy concentration ($\overline{\Delta\alpha}<0$) when the discontinuity has lower velocity than the surrounded media. On the contrary, energy decays ($\overline{\Delta\alpha}>0$) are present when the contrast between the materials is opposite. For the field case, results were also very representative, and discontinuities were effectively identified.
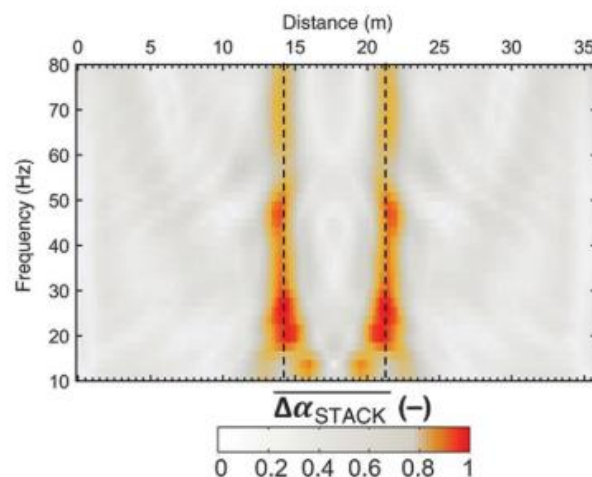

Figure 11. Attenuation coefficient results for stacked absolute negative and positive values on the same heterogeneity shown before for the other methods. Extracted and modified from Colombero et al,. (2019)

2.6.4 Autospectrum

This method was developed by Zerwer et al., (2005) to study the use of Rayleigh waves dispersion for the detection of surface cracks in concrete structures. The autospectral density G_i is defined as the sum of the squared real (Re) and imaginary (Im) parts of the discrete Fourier transform of the signal Y_i:

$$G_i(f) = \{Re[Y_i(f)]\}^2 + \{Im[Y_i(f)]\}^2 \qquad (8)$$

The computation of the energy as a function of the frequency is done within specified frequency intervals and represents an alternative way to display the energy content of every CSG (Colombero et al., 2019). Zerwer et al., (2005), found that transmitted energy of Rayleigh waves decreases in the presence of a slot. A qualitative estimation of the depth is also possible due to the property of the cavity to effectively block the wave propagation.

- Bergamo & Socco, (2014) applied this method to both a synthetic and large-scale field data set in which the presence of a fault system was known. The results were consistent whit the those find by Zerwer et al., (2005) in terms of the effective location of lateral inhomogeneities, but not in terms of the estimation of the depth. The authors pointed out that it may be due to the use of single-fold data analysis.

- Colombero et al., (2019) adapted the method to multifold data and found significant improvements. Results showed that when the velocity/acoustic impedance of the targets were lower than the surrounding medium (like cavities), high values of autospectral were clearly observed and located inside the bodies (Figure 12a). On the contrary, when the anomaly has higher velocity (like an intrusion), higher values were observed outside the target, finding some difficulties to estimate its exact location (Figure 12b).
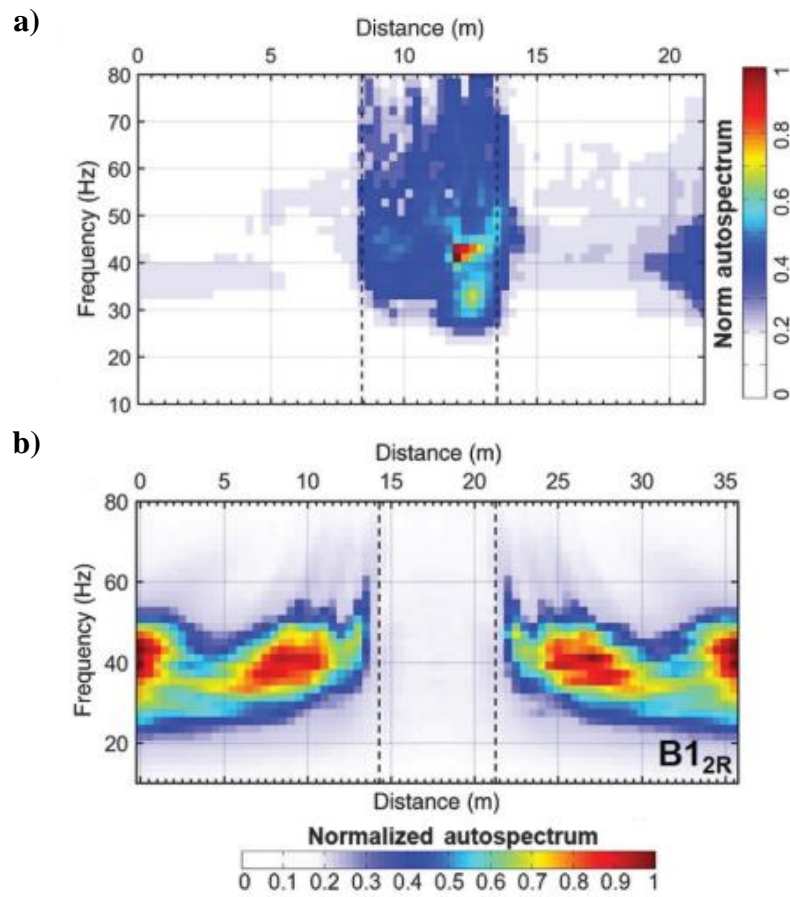
Figure 12. Multifold stacked autospectrum plots for real and synthetic configuration of a) real low-velocity body and b) synthetic high-velocity intrusion. Extracted and modified from Colombero et al., (2019).

Chapter 3

Methodology

The methodology proposed in the present work for seismic data processing is based on the implementation of computational tools to assess geophysical characterization of embankments. Two different approaches will be compared: classical refraction tomography and the fast effective four SW-methods proposed by Colombero et al., (2019). The methods are applied to landstreamer data for the evaluation of the effectiveness in monitoring of embankments. The interpretation will be performed focusing on the location of the pipeline within the embankment.

The computational methods used in this work to assess SW analysis are based on the methodology followed by Colombero et al., (2019)

To apply the methods to landstreamer data for embankment characterization, some optimizations are however explored and proposed within this thesis. In particular, to

reduce the effects of the variation of the source energy along the investigated line, the traces of each shot are normalized, by dividing the amplitude of each trace of the CSGs by the maximum amplitude of the trace closest to the source. This normalization ensures that each landstreamer position is imaged with the same energy and, while stacking or assembling all the line segments, the contribution of each survey position is equalized to avoid misinterpretations. A comparison between computations on non-normalized CSGs will be shown to better highlight the methodological improvement.

As a further improvement, with the same aim of balancing the different portions of the landstreamer acquisition, the final stacked or merged results are normalized by the coverage of each receiver location along the survey line. This procedure allows to strengthen the information for the line parts where a poor coverage is present and to reduce the misleading high-energy information due to the high sampling of some receiver position. The two optimizations can be seen as two balancing operations, the first is internal to each CSG, the second applies to the whole survey line.

3.1   Presentation of the data

The landstreamer data used in this work were acquired using an array of 24 vertical geophones (4.5 Hz) spaced by 1 m. The data set is composed of 49 and 66 CSGs in the positive and negative offset, respectively. The total surveyed lines for positive and negative offsets are shown in Figure 13, including the ERT by Comina et al., (2020). Data are kindly provided by prof. Comina (Department of Earth Sciences, Unito) and Techgea srl.
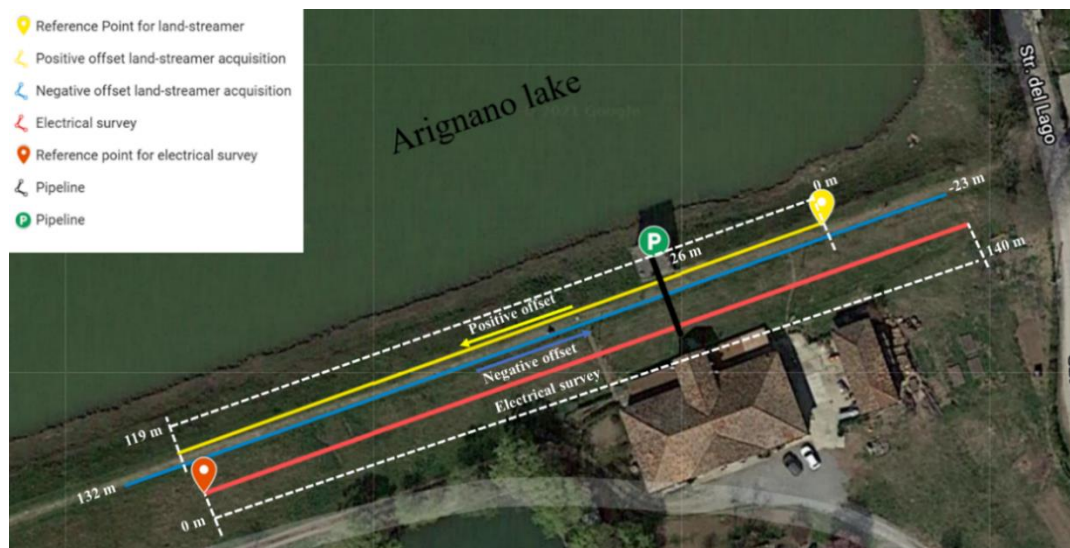

Figure 13. Plan view of the landstreamer positive and negative path. Electrical survey path. Extracted and modified from Google Maps.

The black line, transversal to the embankment, represents the pipeline which is located approximately at 26 m from the 0-reference point (yellow dot, Figure 13). The path of the electrical survey was the same as for the negative offsets, whit a reference point located East (red dot, Figure 13).

It was conventionally decided to refer to positive offsets the line segments having the source located to the East, and to negative offsets the ones having the source on the West, to have a reference system starting close to SE edge of the embankment (reference point, 0 m) and increasing towards SW along the embankment. Figure 14 shows the landstreamer path for 3 different configurations of positive and negative offset.
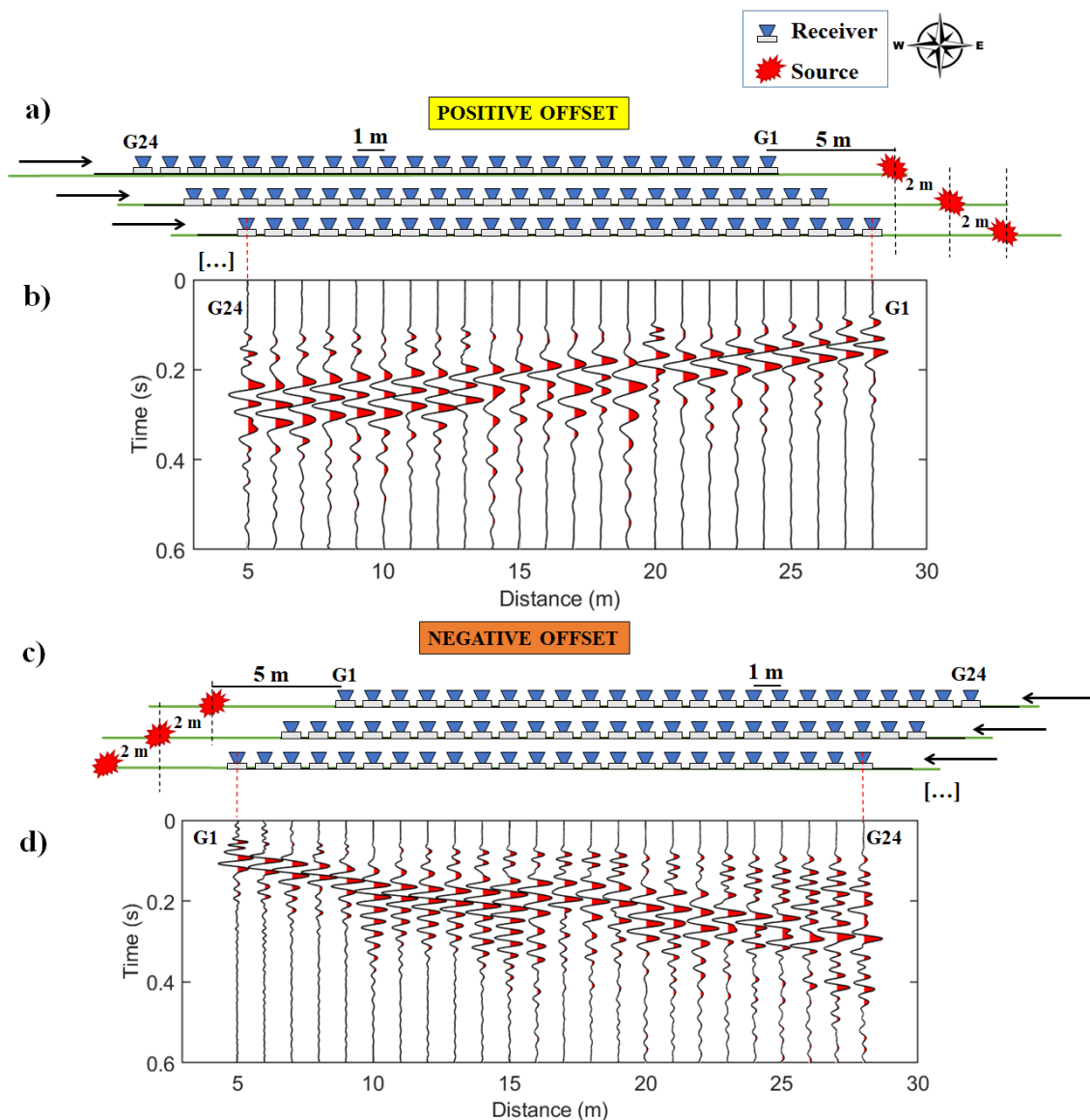
Figure 14. Landstreamer acquisition scheme. a) positive and c) negative offsets. Associated sample CSGs are shown in b) and d).

The first receiver was the closest to the towing vehicle (G1,Figure 14). A hammer (5 kg) impinging on a metallic plate by an operator was used as a source for each landstreamer position. The source was located at 5 m from the last receiver of the landstreamer (G24, Figure 14).

Acquisition parameters

-   N° geophones: 24.

-   Distance between geophones: 1 m

-   Distance of the source to the survey line (offset): 5 m

-   Spacing between shots: 2 m

-   Trigger time (starting record time before the first shot): 0,03 s

-   Sampling interval: 0.5 ms

-   Recorded time: 1 s

Positive offset acquisition

The last geophone of the survey line in the first shot was located at a 0 m reference point (Figure 15). Geophones were located at 1 m distance. For the next acquisitions, geophones were moved 2 m from the initial position until the last position of the last geophone was equivalent to 96 m.
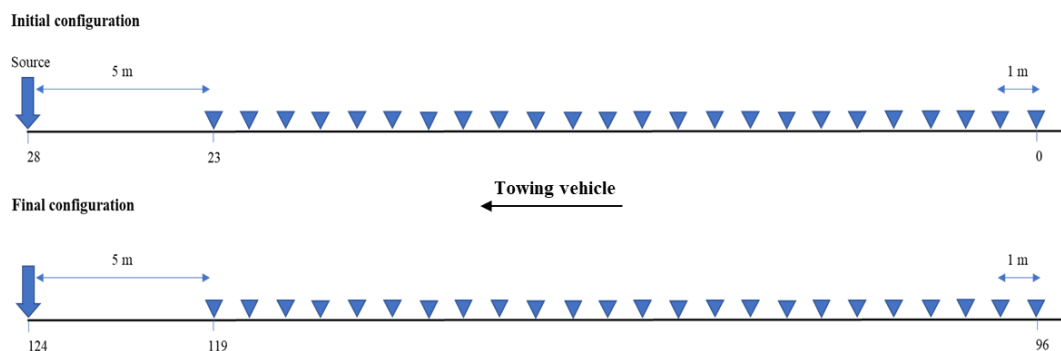

Figure 15. Initial and final configuration of the survey line for the positive offset.

Negative offset acquisition

The acquisition started by positioning the source at 92 m from the same reference point of the positive offsets (Figure 16). The acquisition was made following the same geometry of the positive offset. The final position of the source is at -38 m from the reference point.
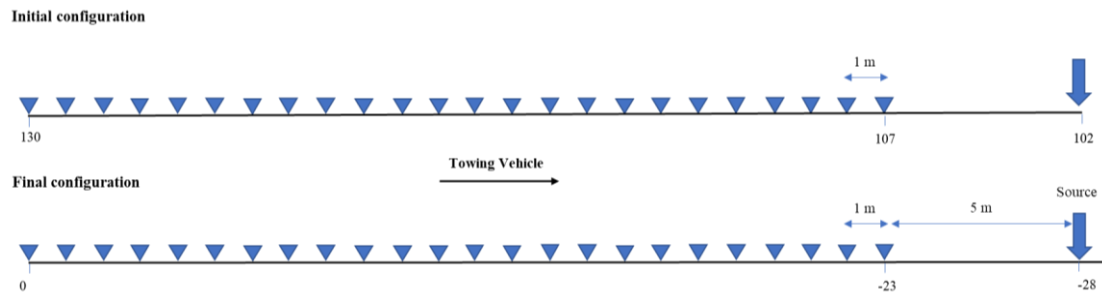
Figure 16. Initial and final configuration of the survey line for the negative offset.

3.2   Refracted wave analysis

In the refracted wave analysis, the focus is on selecting the arrival time of P-waves, which have the property of being the first to be recorded due to its higher velocity, so the travel time is easy to recognize as the first perturbation in the trace (see Figure 17). The selected travel times and the position of every geophone are the input data for the generation of the velocity model. The software uses the travel times to calculate velocities and to provide graphical displays of their variation. For this purpose it was used the standard inversion procedure of the software GeoTomCG, version 4.0 (GeoTom, 2014).

A Matlab code was used for the selection of the first arrival times of P-waves. This code enables the CSG visualization, with a time-domain graph having the receiver number or position in the X-axis and the arrival times in the Y-axis of all the waves recorded by the seismograph. The response of every wave is transmitted and displayed for each geophone in terms of traces, showing different amplitudes, frequencies and arrival times that allow to distinguish the type of wave.

3.2.1 First arrival picking using MATLAB code.

The code is developed to read a Matlab extension file that contains all the traces of every geophone in the CSGs, plus the following information:

- Normalized traces.

- Distance of every geophone from the source, expressed in m

- Distance of every geophone from the reference point, expressed in m

- Distance of the source from the reference point, expressed in m

As is shown in Figure 17, the arrival times of the P-waves are selected manually and plotted in green. Travel times are increasing with offset and the highest value is recorded by the geophone positioned farther from the source.
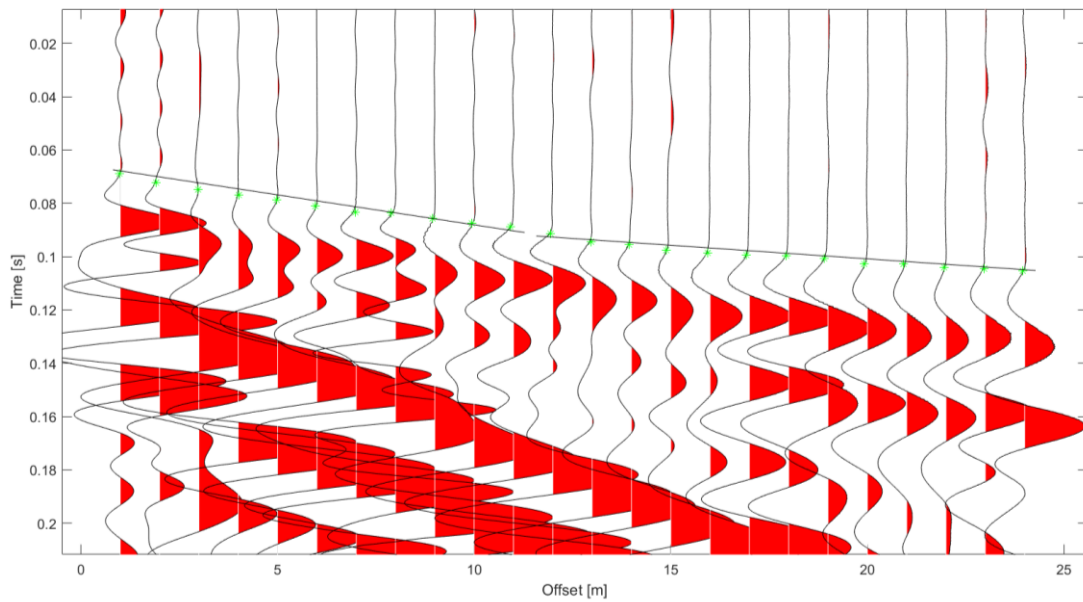
Figure 17. Display of a CSG. Extracted from Matlab.

For each CSG, the code generates a new extension file containing an array of three columns: 2 columns with the position of the source and the geophones from the reference point in m, and a third column with the selected arrival times in s. This data will be used as input data for the generation of the velocity model.

3.2.2 Velocity model using GeoTomCG.

The velocity model was generated using only the CSGs with positive offset, for which already 1176 first arrival times where picked (49 CSGs, 24 traces). The steps to generate the velocity model are described as follows:

a) **An extension of the GeoTom input file ".3dd" is required. This input file begins with two rows containing text and the header. Then, there is an array of 8 columns with the following information:**

   1. Number of the row.

   2. Position of the source in X in m

   3. Position of the source in Y ($y\neq0$ for 3-D models).

   4. Position of the source in Z ($z\neq0$ for 3-D models).

   5. Position of the geophones in m

   6. Position of the geophones in Y ($y\neq0$ for 3-D models).

7. Position of the geophones in Z (z≠0, for 3-D models).

8. Travel time in s, this time is corrected by subtracting from the selected time the delay set in the seismograph before starting to record the signal. The trigger delay is equal to 0,03 s.

This input file must be prepared in a standard text document following this strict sequence in order to be correctly read by the software.

b) **Loading the input file in the section "Data" → "Open data file (*.3dd)"**

Once uploaded the input file, the software shows the first 1000 lines in a window with the intention to verify if they were correctly uploaded (Figure 18).

Figure 18. Display of the input data file uploaded in GeoTom CG. Extracted from GeoTomCG.

c) **Generation of a preliminary velocity model in the section "Model" → "Generate model":**

The required inputs are:

- Uniform velocity in m/s, a default velocity is calculated from the input data as a value between the average and the straight-line calculated velocity (Geotom, 2014).

- X coordinates, i.e., the smallest and largest coordinate of the source and geophones along the line.

- Z coordinates, i.e., the smallest and largest depth values for the generate model.

- Number of nodes in every direction. Considered equal to the maximum absolute value of the coordinates in X and Z to improve the interpretation of the data.

Figure 19. Display of input data window for the generation of initial velocity model. Extracted from GeoTomCG.

d) **Open the initial model created in "model" →"open model"→"display model".**
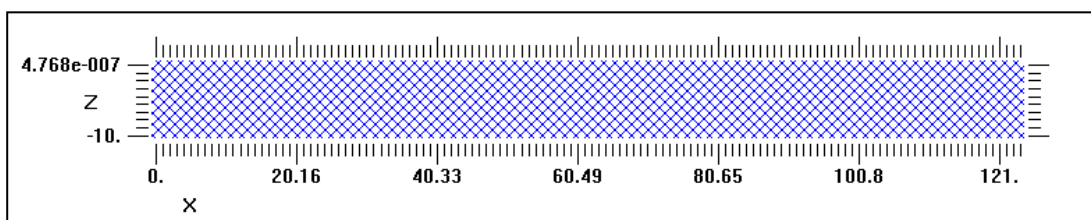

Figure 20. Display of the initial model. Extracted from GeoTomCG.

The initial model showed in Figure 20 represents a uniform grid with a unique velocity and boundaries in X and Z. To improve and adjust it to a more realistic media containing different materials and increasing velocities with depth, the model can be edited setting up a velocity *vertical gradient*.

e) **Create the vertical gradient model in "model" → "edit model":**

In this section, it is required to set up a minimum and maximum velocity at the model minimum and maximum depth. Figure 21 shows the displayed window in this step.

Figure 21. Display of input parameters window for the vertical gradient model. Extracted from GeoTomCG.

The velocities for the vertical gradient were chosen considering the results from two geotechnical surveys made in two different points on the Arignano embankment (Fazio, 2019). Both surveys reached a depth of 15 m and allow to know the stratigraphic condition of the material composing the embankment, which is in overall backfill material of silt and clay for the first meters, silky and sandy clay material while depth increases. (Figure 22).

The knowledge of the type of material eventually conducted to estimate the velocities for the vertical model, based on the information in literature about velocity of P-waves for different materials (Table 1)
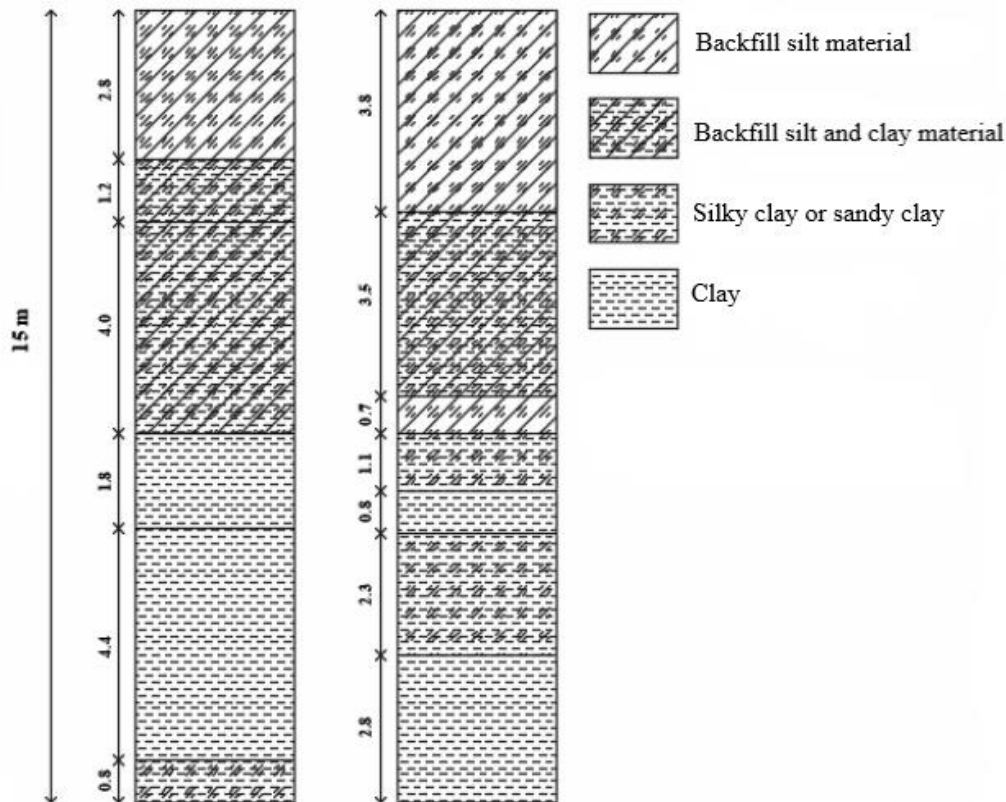
Figure 22. Stratigraphy of two different points of Arignano embankment. Extracted and modified from Fazio (2019).

Table 1 Refence values of P waves velocities and resistivity for different materials. Recovered and modified from SEGwiki.com and Ramirez, (2011)

Material	Velocity [m/s]	Resistivity ρ [Ωm]
Unconsolidated materials		
- Sand (dry)	200 – 1000	10 – 100
- Sand (water saturated)	1500 – 2000	-
- Clay	600 – 2500	20
Pore fluids		
- Air	300	-
- Water	1400 – 1500	0
Other materials		
- Steel	6100	-
- Concrete	3600	-

Once the vertical gradient model is created (see Figure 23), the software is prepared to run the inversion through a *standard inversion* mode. For that, the number of straight and bending ray iterations, as well as the minimum and maximum allowed velocity for the inversion are required:
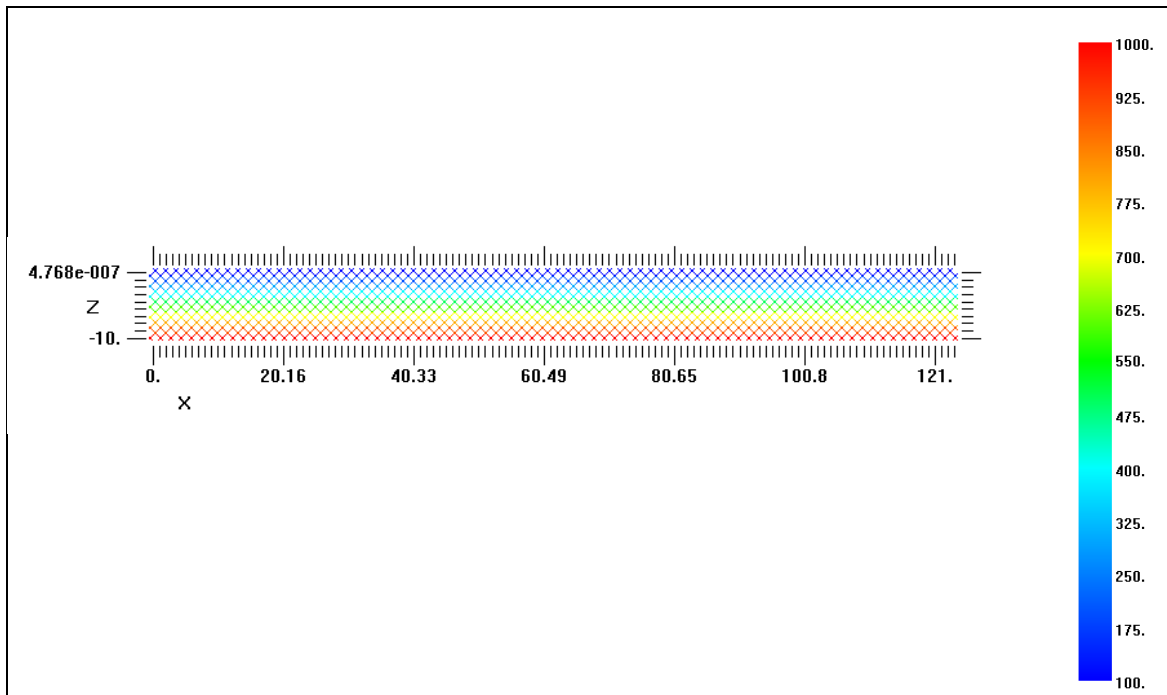
Figure 23. Display of the vertical gradient model. Extracted from GeoTomCG.

f) Set the inversion parameters: "Options"→"Inversion parameters":

Inversion parameters needed are listed below, Figure 24 illustrates the window displayed by the software.

- Number of straight-ray iterations: allowed range goes from 5 to 10.

- Number of bending-ray iterations: allowed range goes from 5 to 10.

- Minimum and maximum allowed velocity.

Figure 24. Display of input inversion parameters window. Extracted from GeoTomCG.

g) **Run the inversion: "Run"→"Run standard inversion".**

For the inversion, the software works with a *standard inversion*. First with a number of straight-ray iterations and then with a number of bending-ray iterations given by the operator. The evolution of the inversion is shown by displaying the RMS residual and Sum residuals for every straight and bending iterations performed. When the final iteration is done, the software generates a ".rsd" file that contains the residual for every ray path (Geotom, 2014). Residuals are the difference between travel times extracted from every CSG and the times of the waves traveling through the media calculated by the software.

3.3 Surface wave analysis

Surface wave analysis explore strong concentrations or decays of the energy. The input data for these methods are the same used for the refraction tomography and methods are applied to both positive and negative offsets data. All computations are developed in MATLAB codes.

The analysis focus on the detection of strong anomalies along both landstreamer profiles, and stacked plots will be generated to improve the quality of the results. The knowledge of the presence of the pipeline within the embankment represents an excellent target due to the significant contrast between the loose material of the embankment, the concrete structure containing the pipeline and the inner empty space. The verification of the location of this target through SW-methods may corroborate the effectiveness of these techniques for their

quick application during a seismic acquisition and to assess the integrity of embankments as an economical solution of diagnosis.

The following sections will describe the methodology followed to process negative and positive offset data of the four SW-methods: computation of energy, energy decay exponent, attenuation coefficient and autospectrum.

3.3.1.   Energy E_i

The computation of energy was performed using a MATLAB code capable of reading every CSG file containing the normalized traces and the position from the reference point of the source and geophones. In addition to this, the code requires a vector *r* that contains the distance of every geophone from the source. This vector represents the function that will be used for the geometric spreading correction and is constant for all CSGs.

The process starts with the calculation of the energy E_i on each trace in the CSG as a function of the signal amplitude, followed by the geometric spreading correction by multiplying the computed energy for the offset distance *r*, as show in Equation 2. The next step is to calculate the NED parameter using Equation 3, that normalizes every value of energy in the CSG by the maximum value of energy. At this point, the code generates *normalized energy plots* (Figure 25) for every CSG as a function of the geophones distance *r* for positive and negative offsets data.
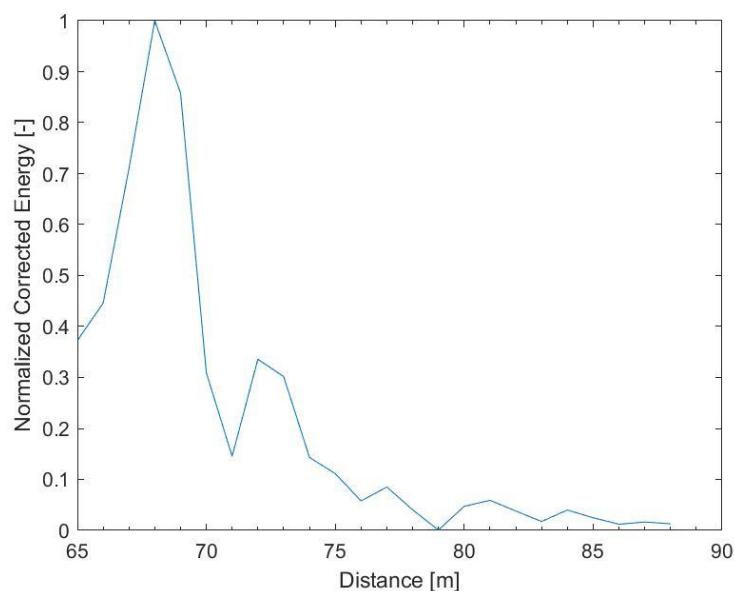

Figure 25. Normalized energy plot for one CSG with positive offset. Extracted from Matlab.

Then, the energy values with the same offset are stacked and normalized again by the maximum value. The result is an *E-r* plot for both positive and negative offset showing the

fluctuations of the energy as a function of the distance from the reference point. The final step is to stack and renormalize positive and negative offsets to balance the coverage along the line, reduce the source influence, and improve the quality of the image.

3.3.2.   Energy decay exponent γ

For this method, the input data are the file containing the energy values E_i calculated in the previous method and the position of the source and geophones. The first step is to create a moving window that will shifts along the traces of every CSG. The length of the window is an input parameter and corresponds to the number of traces considered for the calculation the energy decay exponent γ as the slope of the energy plot, considered in bilogarithmic scale (Equation 4).

Values of γ computed at the same window location (Figure 26) from different CSGs are then averaged, and the standard deviation is calculated. The final result is a γ-r plot containing the γ values of positive and negative offsets.
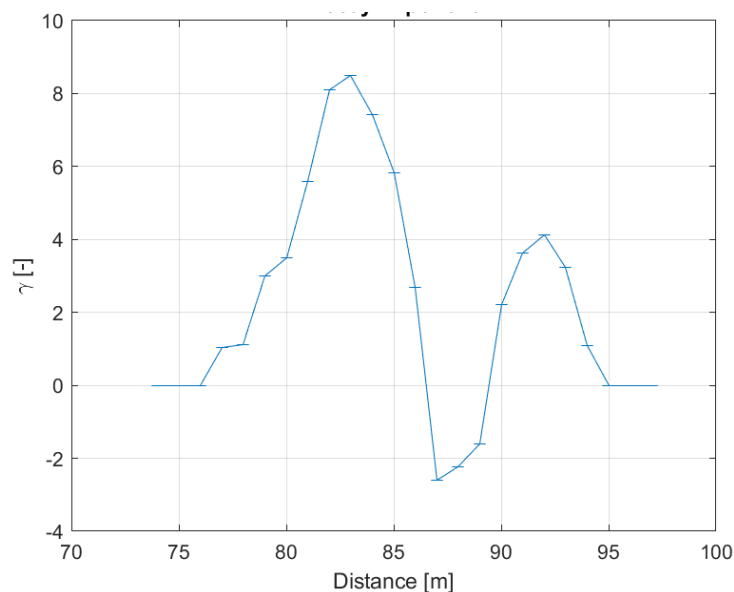

Figure 26. Energy decay exponent values for one CSG with positive offset. Extracted from Matlab.

3.3.3.   Attenuation coefficient α_f

This method evaluates the local attenuation, considering the energy as a function of different frequency components. As for the energy decay exponent, a moving window is shifted along the traces of each CSG. Values of α_f are calculated as the slope of the *E-r* plot with *E* computed for different frequency component in natural logarithmic scale (Equation 5). This operation is done for both positive and negative offsets. Then values are normalized to evaluate strong variations neglecting frequency dependence of each value of α_f using

Equation 6. Eventually, normalized $\alpha_f - r$ plots are generated for positive and negative offset.

In the end, the normalized stacked absolute values of α_f for positive and negative offsets are stacked to emphasize their contribution and improve the visual representation using Equation 7.

3.3.4.   Autospectrum

The computation of the autospectral density G_i is another way to evaluate the energy content considering different frequency bands. For this method, the input parameters are the normalized traces and the position of the source and geophones. The first step is to apply the geometric spreading correction using the same gain function used for the computation of energy. Then, the autospectral density is calculated using Equation 8 as the sum of the absolute values of the real and imaginary parts of the Fourier transform of the signal. These values are normalized, and the result is a $G_i - r$ plot for every CSG as is shown in Figure 27.
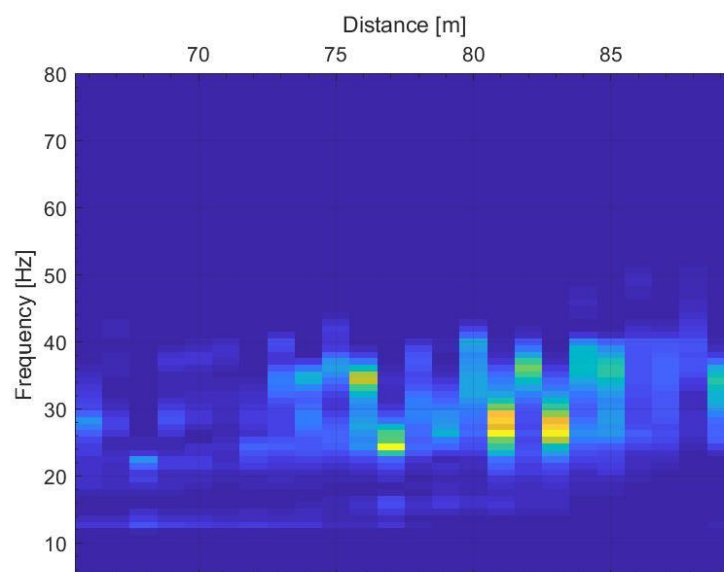

Figure 27. Autospectral density for one CSG. Extracted from Matlab.

As for the other methods, all the autospectrum plots are stacked to improve the readability of the data. The final result is a coverage-normalized positive and negative stacked autospectrum plot whit higher coverage and quality.

A summary of the methodology followed to process negative and positive offsets data of the four SW-methods is presented in the Figure 28.
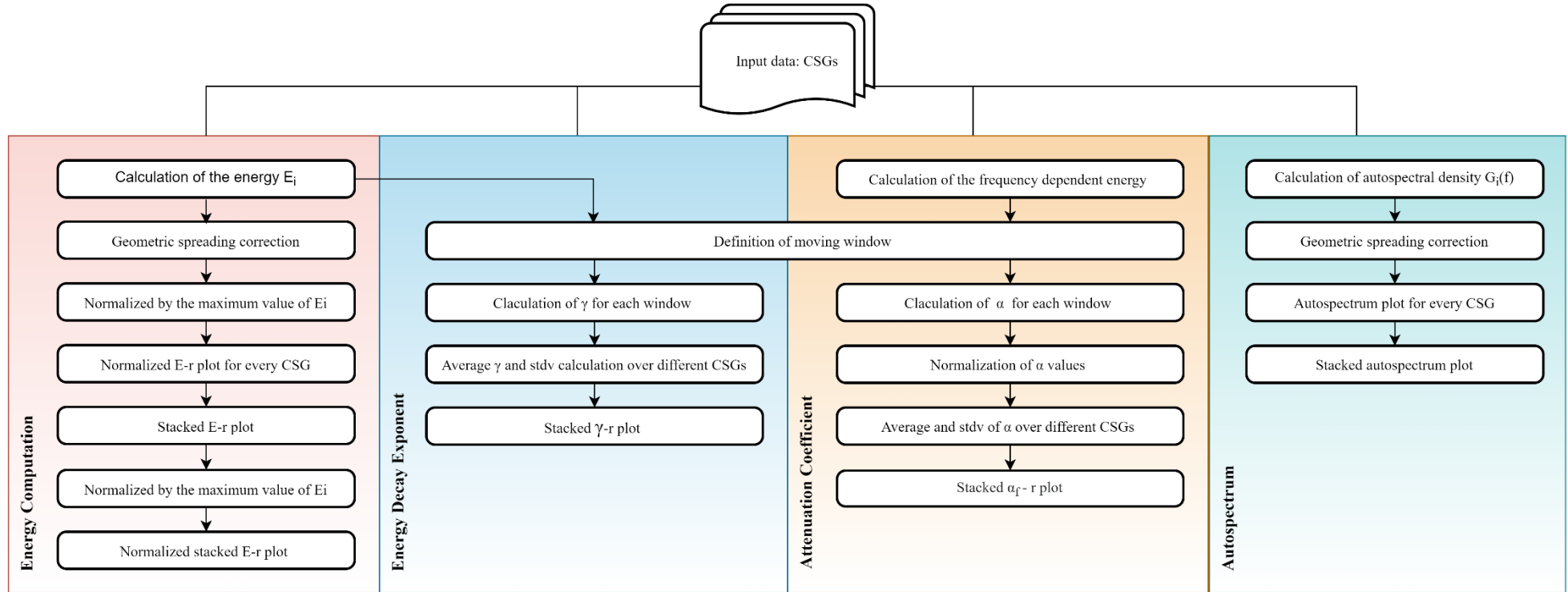
Figure 28. SW- analysis workflow.

Chapter 4

Results and Discussion

The velocity model was generated following the methodology for refraction tomography described in Chapter 3. The interpretation of the model was performed focusing on the location of the pipeline within the embankment. Following the same interpretation approach, the four SW-methods were analyzed in order to locate the response of the pipeline as fluctuations of the energy signal. The response of the pipeline using refraction methods was compare with the results obtained using the four SW-methods.

4.1.   Refraction method analysis

For the generation of the velocity model, 1176 first arrival travel times were selected manually on each of the 49 CSGs with positive offset (24 travel times each CSG). Negative offset data was not used in the refracted analysis to reduce the processing time.

Before the generation of the velocity model, the selected travel times of all the CSGs were plotted together to verify whether if there was a regular tendency in the selected times or if there were any anomalies during the picking process. The software GeoTomCG allowed to plot all CSG together in travel times vs geophone distance curves.
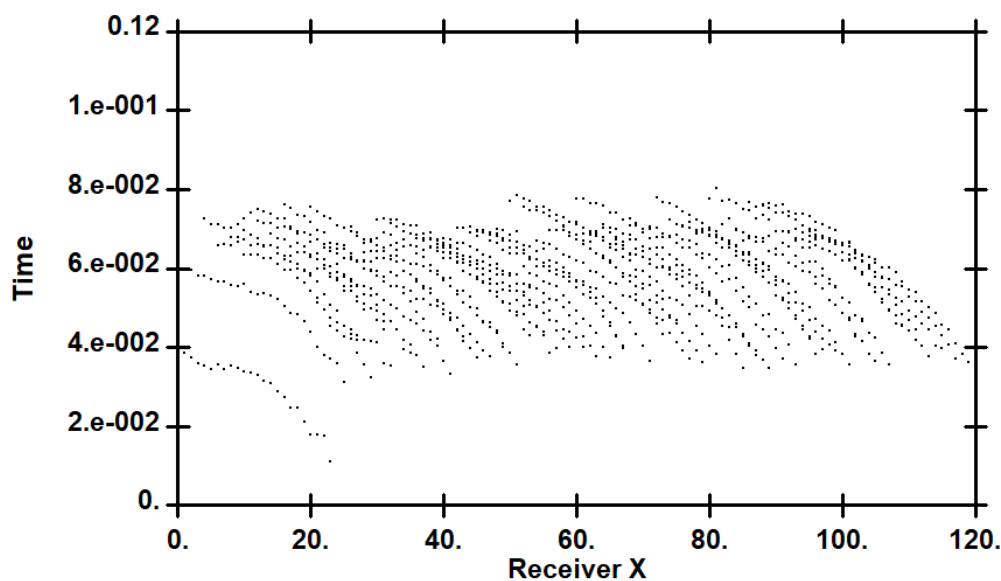

Figure 29. Travel time vs geophone-distance curves of all the CSGs with positive offset.

In Figure 29, there are 49 curves representing the 24-travel time selected for the CSGs. Every point represents the picked time (in s) as a function of the geophone position (in m) along the surveyed line. In general, all CSGs showed a similar trend: decreasing first arrival times when the distance is increasing (i.e. the distance from the source is reducing). Picked arrival times range from 0.04 to 0.08 s.

The first and second CSG showed a different range of picked time values that goes from 0.01 to 0.06 s. For this reason, it was decided not to consider these shots because they could lead to misinterpretations.

4.1.1.   Velocity model parameters

Table 2 shows all the input parameters set up in the software for the generation of the velocity model. For the initial model it was used a uniform velocity of 188 m/s estimated by the software after uploading the selected travel times. This value is between the average and lowest straight-line velocity calculated.

The model coordinates along the X-axis were set from 0 to 120 m, considering the total length of the survey. Coordinates along the Z-axis go from 0 to 10 m depth, considering the high of the embankment and the depth of the buried pipeline. The number of nodes was considered equal to the maximum absolute value of the coordinates in X and Z, resulting in nodes at 1-m spacing along X- and Z-axes.

The next step was to improve the initial model, so it was applied a vertical gradient that goes from 100 to 1000 m/s from 0 to -10 m in depth. These values were considered based on the information in Table 1 about the velocity of P-waves in specific materials.

Table 2. Input parameters for velocity model.

Preliminary model configuration	- Uniform velocity: 188 m/s
	- X: 0 – 124 m; Number of nodes:124
	- Z: -10 – 0 m; Number of nodes: 10
Vertical gradient model	- Velocity of 1000 m/s at -10 m
	- Velocity of 100 m/s at 0 m
Inversion parameters	- Number of straight-ray iterations: 10
	- Number of bending-ray iterations: 10
	- Minimum allowed velocity: 100 m/s
	- Maximum allowed velocity: 870 m/s

4.1.2.   Interpretation of the velocity model

The velocity model is presented in Figure 30. The inversion was run following the standard inversion, with 10 straight-ray iterations and 10 bending-ray iterations, resulting in final

values of RMS residual and sum of residuals of $5.60E^{-03}$ and $6.762E^{-01}$s, respectively. The response of the concrete structure containing the pipeline was expected to be found between 20 and 40 m from the reference point and at a depth of about 2-4 m.

The most notorious remarks in the velocity model are summarized as follows:

- A vertical velocity gradient is observed from 20 m to 120 m along the line, P-wave velocity ranges from values below 300 m/s in the first 3 m of depth and then increases up to 870 m/s.

- In the horizontal direction, there is a shallow higher velocity anomaly that persists for the first 20 m of the line and has a thickness of at least 3 m. This anomaly showed a lateral velocity gradient that starts with values higher than 400 m/s in the first 20 m and then decreases to very low velocity values after this distance (<300 m/s). The fact that this anomaly could correspond to the presence of the pipeline was out of consideration because the position of the structure is known to be after 20 m from the beginning of the survey line and at 2 to 4 m depth. Geological information to be correlated with this shallow anomaly are unknown.

- Beneath this shallow anomaly, another anomaly was found with a semi-ellipsoidal shape with a thickness of 5 m starting at 3 m depth; it persisted in the horizontal direction for about 30 m from the reference point. Velocities in this section are about 300-500 m/s (in correspondence with the empty pipeline) and increase laterally. As a consequence, the high velocity layer with velocities higher than 800 m/s shows a marked lateral step around 25 m and seems significantly deeper at the beginning of the line.

- Going further in the model, the first layer within 4 m depth showed an almost regular velocity around 200 m/s. As it went deeper, the velocity increased in a more irregular way from 400 to 800 m/s allowing the distinction of at least 3 layers. There is no information or geological background available to explain these irregularities, but they can be explained with a higher degree of compaction of the embankment material. Very loose clayey materials at the top are characterized by extremely low velocities that progressively tend to increase with depth.
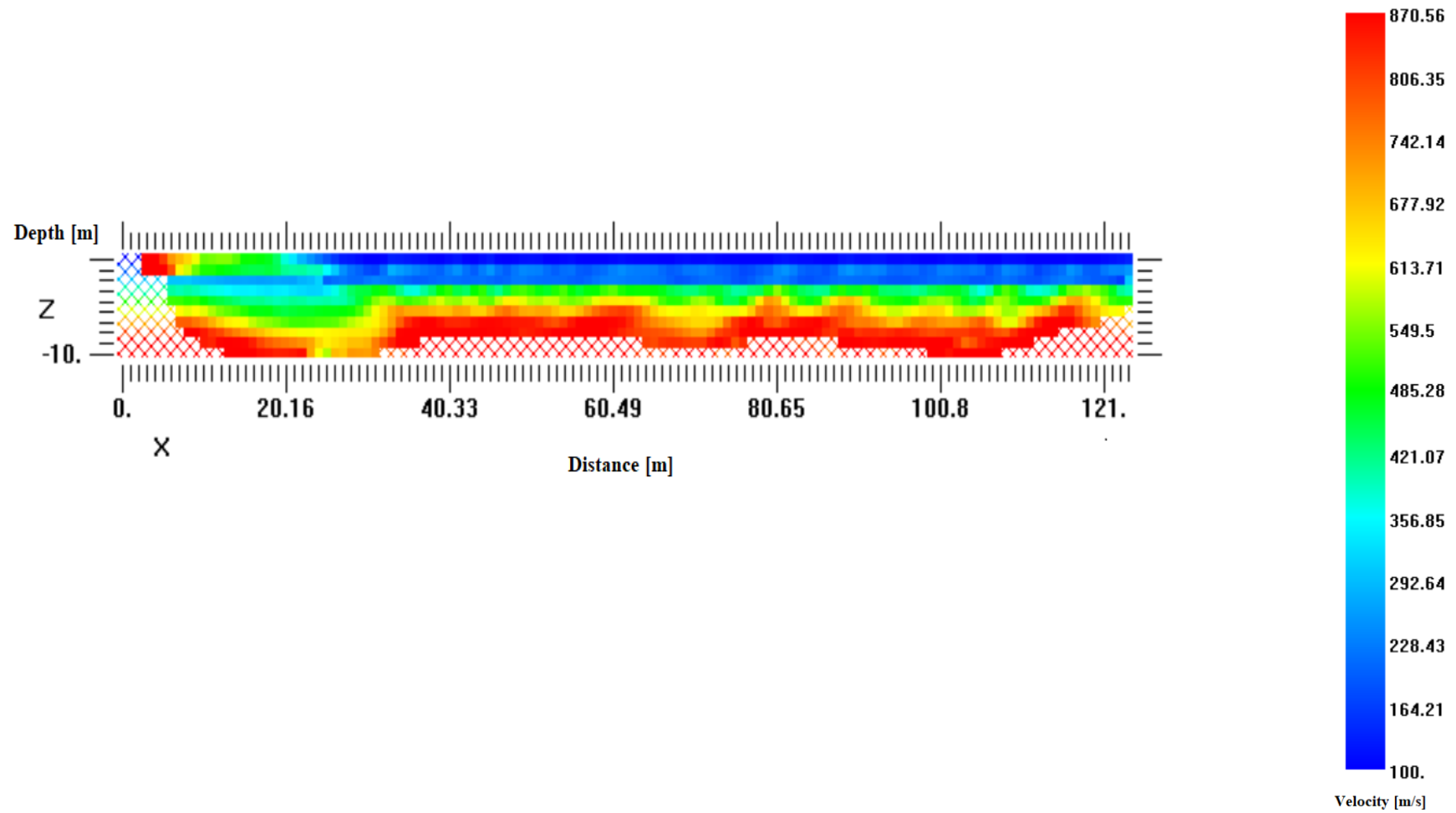
Figure 30. P-wave velocity model generated with GeoTomCG.

4.2.   Surface wave method analysis

Observations presented in this section are based on separate analysis for positive and negative offset data. In the end, results will be stacked and correlated for a final interpretation.

4.2.1.   Coverage

Figure 31 shows the stack of positive and negative offset line coverage. The green region, that goes from 20 to 100 m, delimitates the line segment with equal coverage, meaning that all the receiver positions within the green region registered the signal 25 times. Stacked results are however presented in the range between 0 -120 m, and they are normalized by the total coverage. The interpretation was focused on the 20 - 40 m region where the location of the pipeline and the concrete structure was known to be.
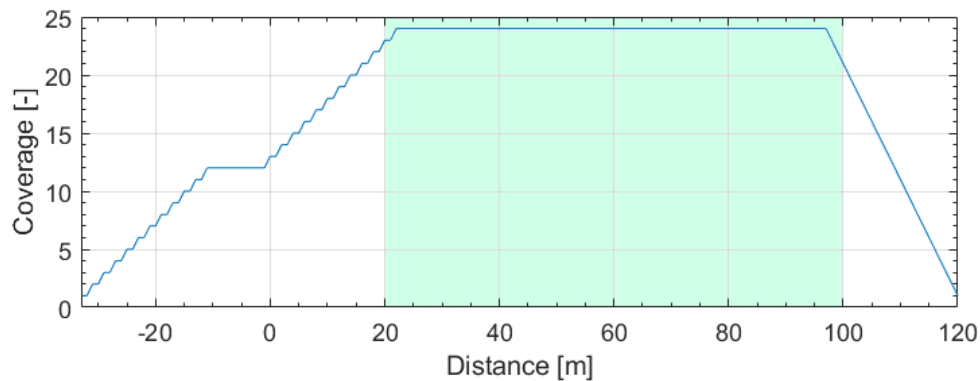

Figure 31. Coverage of the stacked positive and negative offsets.

4.2.2.   Energy, E_i

For each shot, an energy plot was generated, in which the effect and location of the source was more evident (Figure 32). For positive offset plots, the source was located at the end of the plot, for negative offset instead, the source was located at the beginning. Different energy concentrations and decays were however present farther from the source, related to localized anomalies that lately were stacked to improve the total response of the survey line.
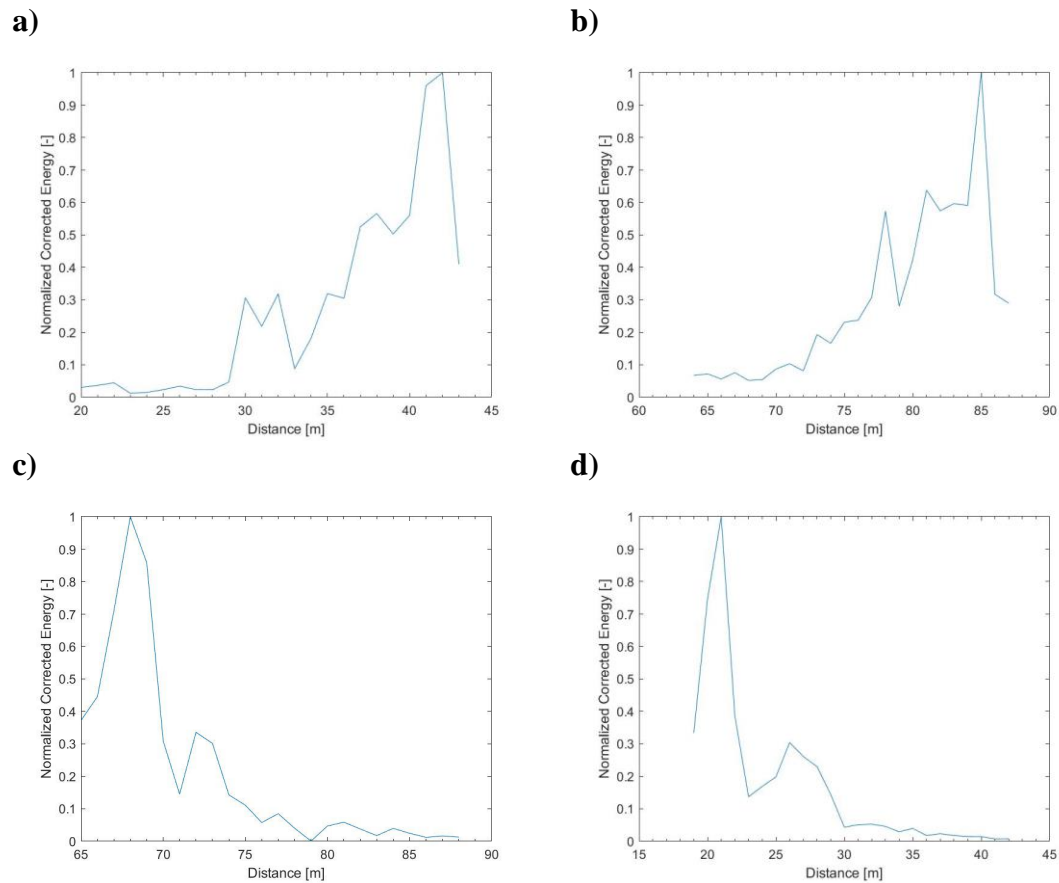
a)

b)

c)

d)

Figure 32. Single shot normalized energy plots for positive (a and b) and negative (c and d) offsets shots.

Then, plots for positive and negative offset were stacked to check the separated responses. The coverage-normalized energy plot for positive offsets is presented in Figure 33. The energy starts to increase after 10 m and then was concentrated mostly within values of 0.1 and 0.3, with some peaks over 0.3 to 0.5. For the negative offsets (Figure 34) the energy was concentrated mostly within 0.2 and 0.5. Energy values showed more oscillations with some peaks over 0.5 to 0.8.
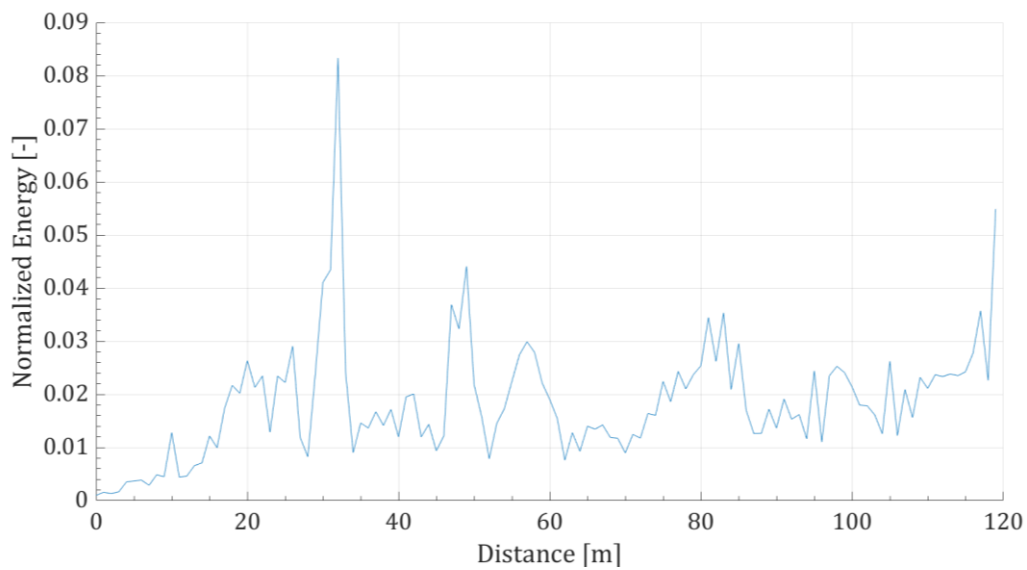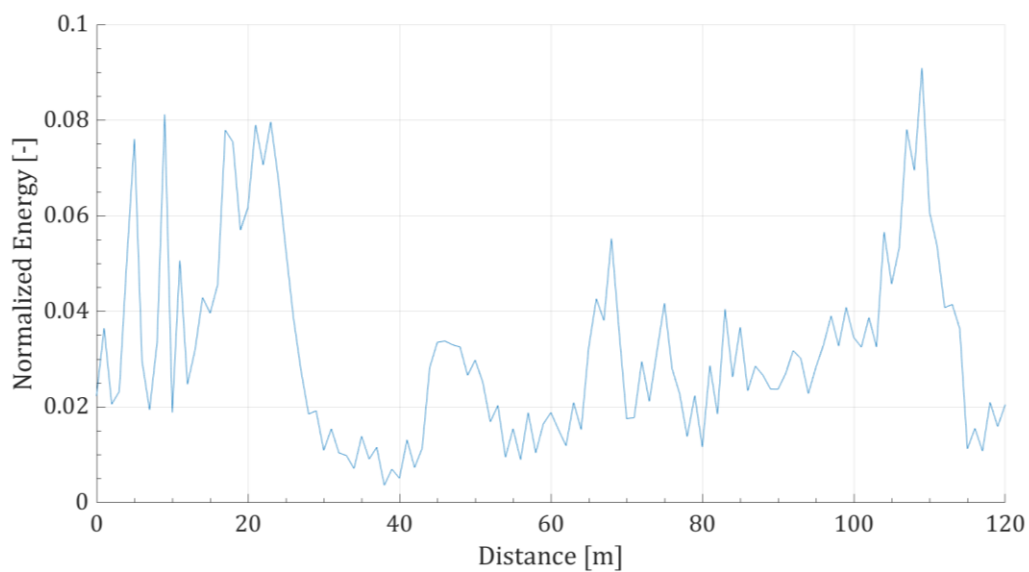
Figure 33. Normalized Energy for positive offset data.

Figure 34. Normalized Energy for negative offset data.

In the positive offset energy plot, the effect of the pipeline presence is clearly represented around 30 m, where the highest concentration of energy is present, this behavior matches perfectly with the results obtained by Colombero et al., (2019) for low-velocity bodies surrounded by a higher velocity material. For negative offsets instead, a significant energy response appeared in the first 25 m, where a low velocity anomaly was depicted by refraction tomography down to 7-m depth, laterally increasing to velocities higher than 800 m/s. Then, the energy abruptly decays, and no clear energy peaks related to the pipeline presents are found in the data. Negative offset trend could be partially influenced by the different

materials in which waves are propagating: the most part of the energy seems to be trapped within the low-velocity anomaly and no clear energy concentrations highlight the pipeline presence.

4.2.3. Energy decay exponent, γ

For positive and negative offsets, the energy decay exponent was calculated following Equation 4, as the slope of ED plot inside the shift window in bilogarithmic scale. Values were presented in -γ vs r plots to match maximum values with energy concentration and minimum values with energy decays.

First, all the values of γ-r single shots were plot together to see the response of each one. Results are presented in Figure 35 and Figure 36 for positive and negative offsets, respectively.
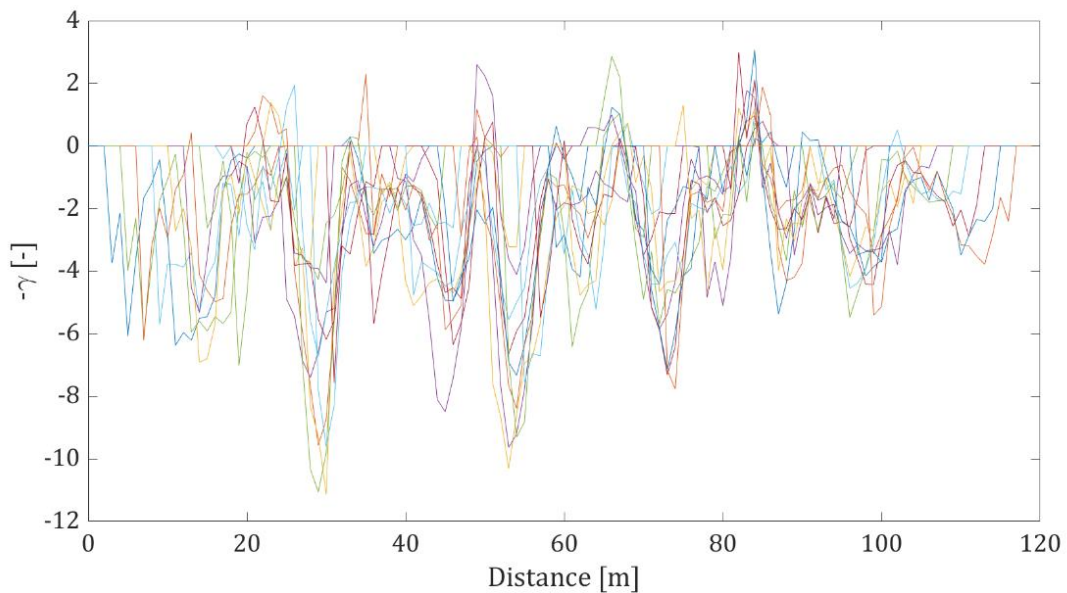

Figure 35. Energy decay exponent for single shots plotted together for positive offsets.
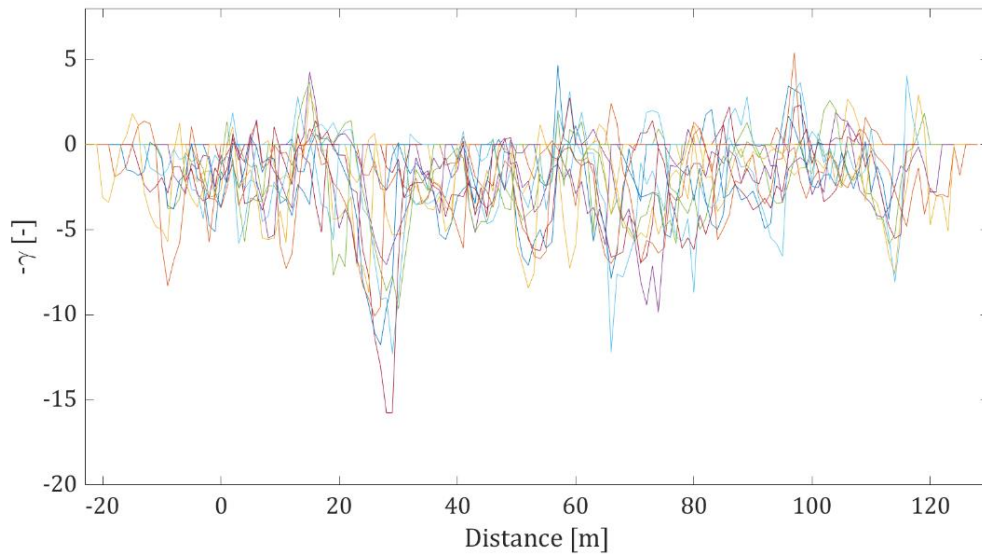
Figure 36. Energy decay exponent for single shots plotted together for negative offsets.

Overall, energy values exhibited the same trend in most of the points with the same offset. The response of the pipeline in both plots corresponds to an abrupt energy decay centered around 30 m. These behavior was maintained after the stacked average of -γ values for positive and negative offset and the calculation of the standard deviation for values with the same offset is included in Figure 37 and Figure 38.
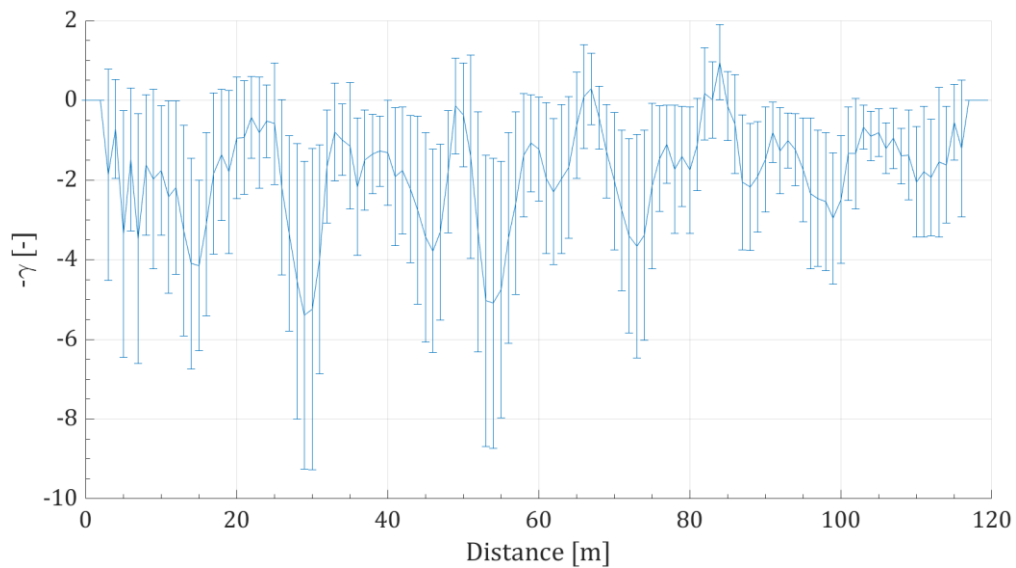

Figure 37. Average energy decay exponent for positive offsets. The error bars show the standard deviation.
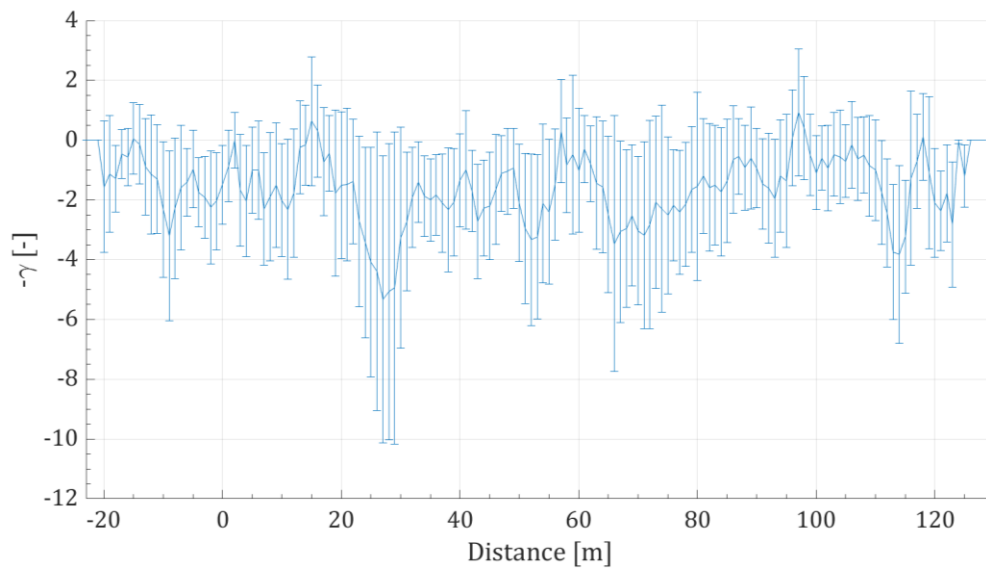
Figure 38. Average energy decay exponent for negative offsets. The error bars show the standard deviation.

For both plots, values of energy decay exponent oscillated between -10 and 2. Positive and negative plots showed the effect of the different materials present within the embankment:

- The positive offset plot showed energy decays within 25 and 35 m, as a response of the energy decay when passing from a low to high velocity material such as the empty pipeline structure and the embankment material on the right side.

- The negative offset plot showed energy decays again, but slightly shifted towards left, maybe resulting again from the wave propagation from a low to a high velocity material, such as the empty pipeline structure and the embankment material on the left side.

Even though both plots have the most notorious anomaly within 20 and 40 m, discrepancies could be related to the fact that the energy decay depicted by the different offsets is located at the two edges of the pipeline structure.

4.2.4.   Attenuation coefficient, α_f

Attenuation coefficient values were computed for different frequency components following Equation 4, then normalized using Equation 5 in order to represent better the different variations of the different frequencies, considering statistical parameters within the moving window. Results for normalized stacked positive and negative plots are presented in Figure 39 and Figure 40 respectively. Values of α_f were reported as a function of the frequency and distance. The frequency band considered was from 10 to 60 Hz.
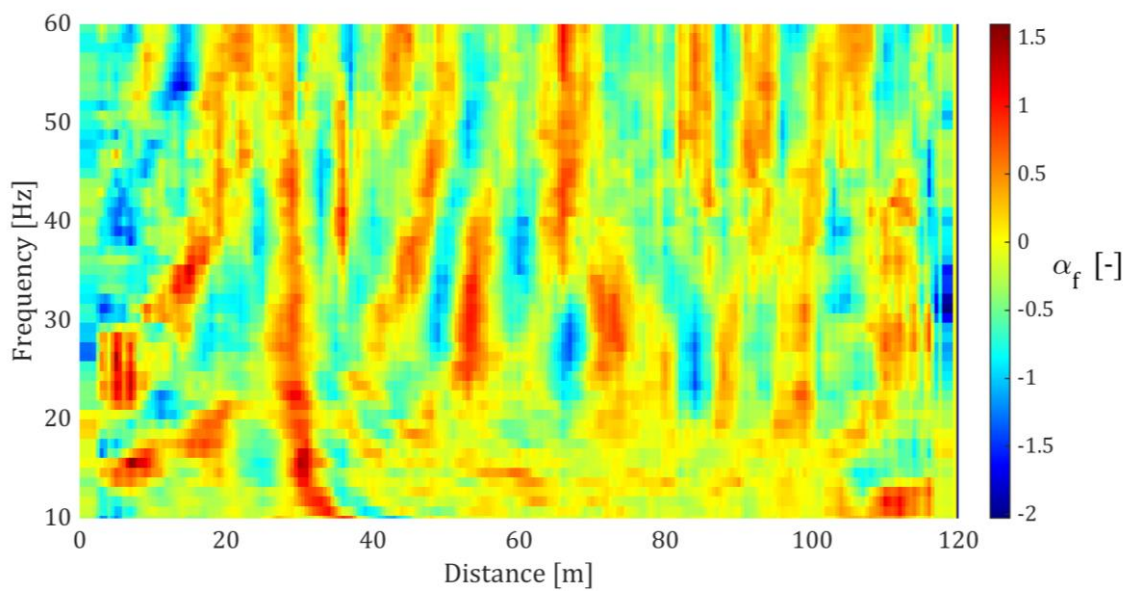
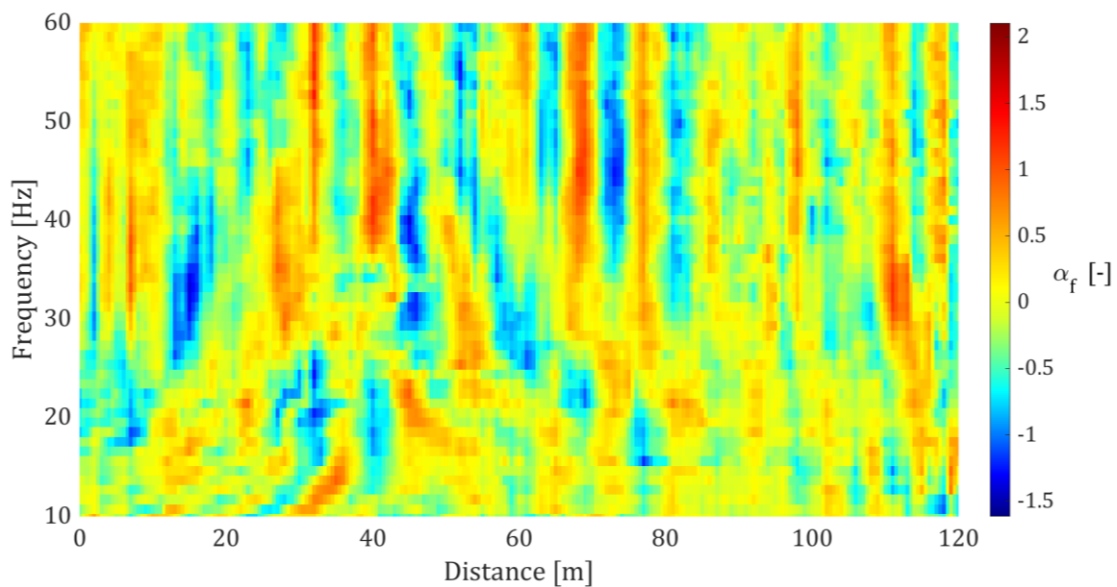*Figure 39.Attenuation coefficient results for positive offsets.*

Figure 40.Attenuation coefficient results for negative offsets.

In general, positive and negative offsets plots showed multiple variations along the profile. Both plots presented alternations between low and high attenuation coefficients values moving on the horizontal direction (or energy concentration and decay). There was also an approximated correspondence in the alternation of energy concentration and decays between positive and negative offset for equal points of the survey line.

For positive offset, the response of the pipeline was clearly depicted with strong values of α_f (energy decay) around 30 m in all the frequency band of 10-60 Hz. For the negative offsets instead, the anomaly had a similar response, but less sharpen than for positive offsets. In both plots, the effect of the energy passing from a low-velocity to high-velocity material (empty pipeline and material of the embankment) was depicted.

4.2.5.   Autospectrum

The spectral density Gi(f) was obtained for every CSG using Equation 8. Then, all shots were stacked and normalized to the line coverage. Results from positive and negative offsets are presented Figure 41 and Figure 42. The frequency band considered was the same of the attenuation coefficient, from 10 to 60 Hz.
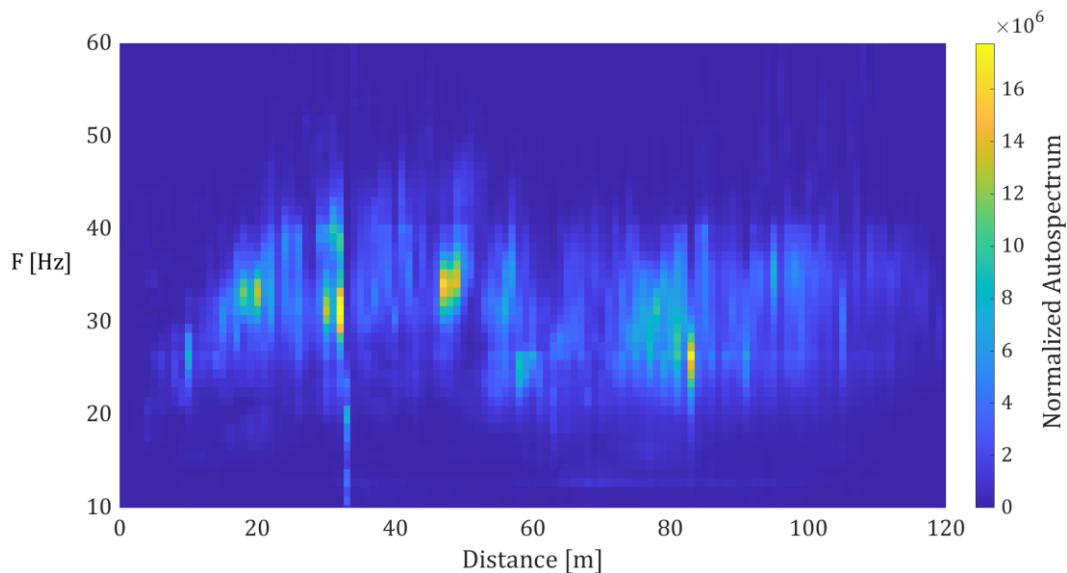

Figure 41. Autospectral density for positive offsets.

For positive offset normalized autospectrum plot, around 30 m, strong values of autospectral density are clearly obtained, covering a wide frequency band. Strong values were in agreement with the results obtained by Colombero et al., (2019) for targets with a lower velocity than the surrounding material, such as the empty pipeline..
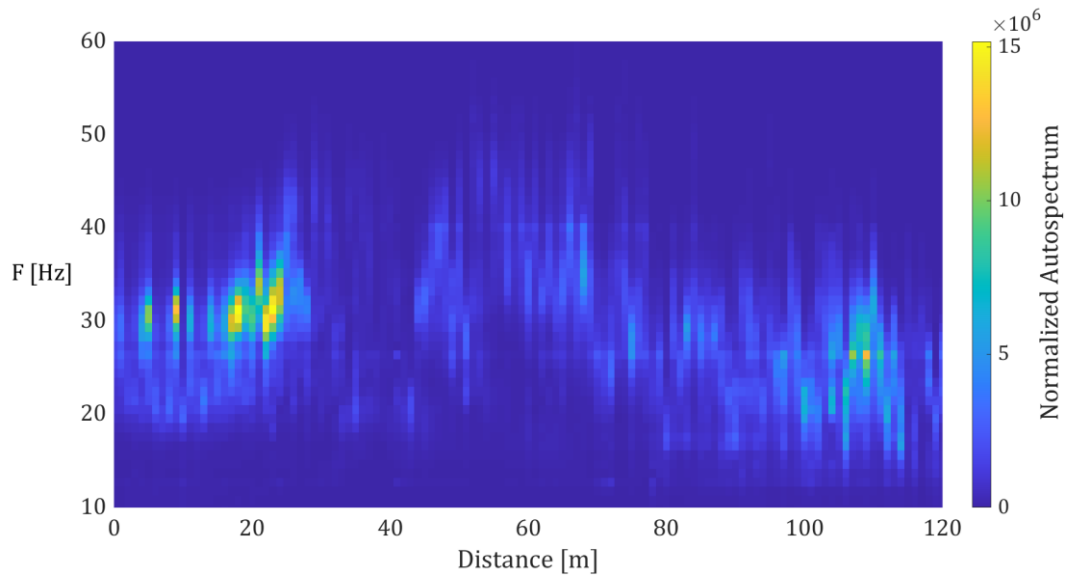
Figure 42. Autospectral density for negative offsets.

For negative offsets, the strongest autospectral response is located before 25 m. The causes may be related to the same reasons of negative offset energy results (Figure 34), i.e. the deepest low velocity anomaly in the first line segment.

To verify the improvement introduced by trace normalization, the autospectrum method was applied to the data with positive offset without normalization. Results are shown in Figure 43. The effect of the pipeline is clearer in the normalized plot than in the one without normalization. Redundancy and normalization of the data sharp and improve the response (compared Figure 41 with Figure 43).
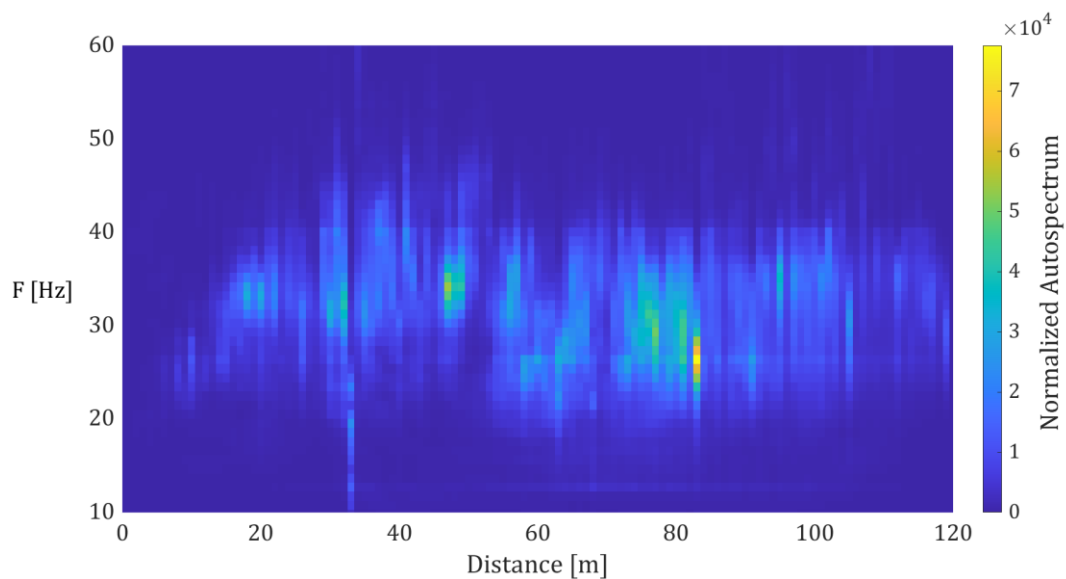

Figure 43. Autospectrum results for positive offset without normalization of traces.

4.2.6.   Correlation of the data

The stacked plots for all the four SW-methods are reported in Figure 44. In the energy plot, the pipeline is clearly depicted, with the highest and sharpest peak of energy located around 30 m (Figure 44a). For the energy decay exponent (Figure 44b), both positive and negative offset curves indicate a clear decrease of the exponent before and after the target. These negative peaks (i.e. energy decay) are shifted of around 3 m, a length approximately corresponding to the diameter of the pipe. Attenuation coefficient from positive and negative offsets were stacked (Figure 44c), but not in absolute values, due to the very limited shift between positive and negative offset results, as already noticed for the energy decay exponent. Results show a maximum of attenuation at the pipeline location, in agreement with energy decay exponent curves. Strong values of autospectral density were also found in the stacked autospectrum plot (Figure 44d), as already obtained from the energy results. The response of energy and autospectrum was therefore found to be in line with past literature applications: energy concentrations are found within the low-velocity anomaly (empty pipeline). Energy decay exponent, however, did not show any energy concentration before the location of the pipeline edges (compare with Figure 10). By contrast, all the exponents were found to become increasingly negative towards the center of the pipeline. The opposite response of the attenuation coefficient at the two edges of the pipeline was also difficult to depict, possibly due to the reduced size of the target.

Despite these minor issues, all the methods were able to identify and locate the pipeline along the line. The results also suggest significant geological and/or geotechnical contrasts in the embankment material. As an example, the low velocity anomaly depicted from refraction tomography in the first 25 m of the reference line is associated to high energy and autospectrum values, an opposite behavior between positive and negative offsets is found in the energy decay exponent and a local attenuation maximum is present at the same locations. At the same time, minor fluctuations in the four seismic parameters after the pipeline location, seem to mirror the morphology of the high velocity materials found below 5 m depth. In particular, for energy and autospectrum results, when the depth of this layer becomes locally deeper, minor peaks are found in the stacked results (e.g. around 80 m and 110 m).
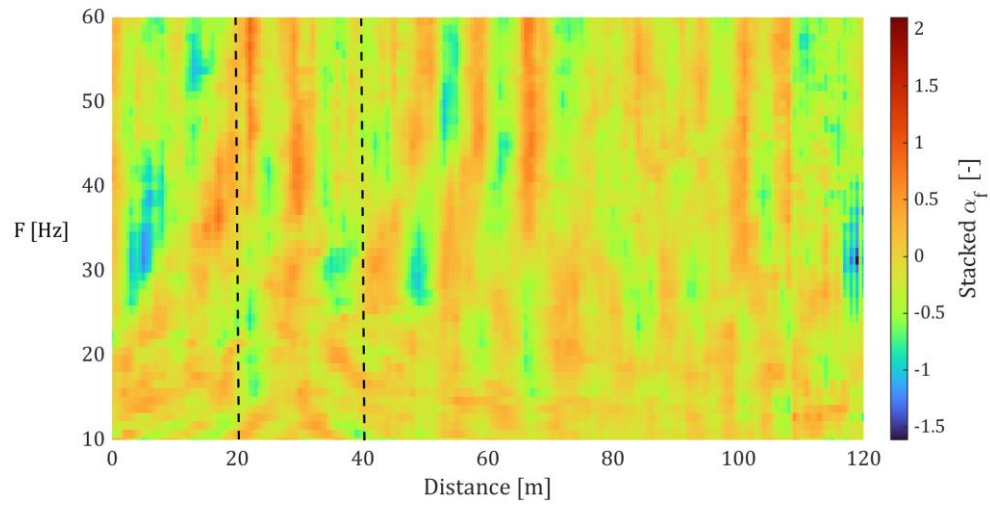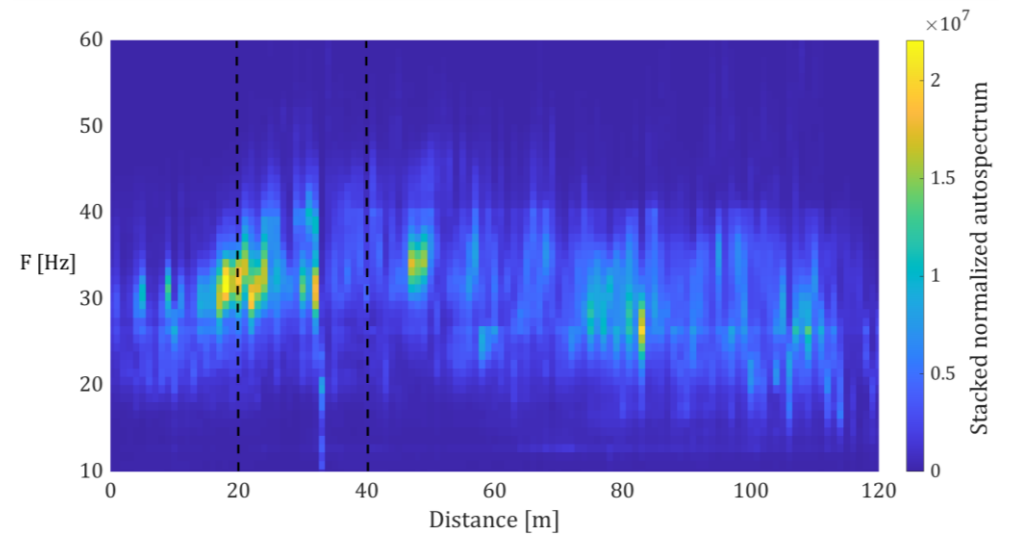
a)
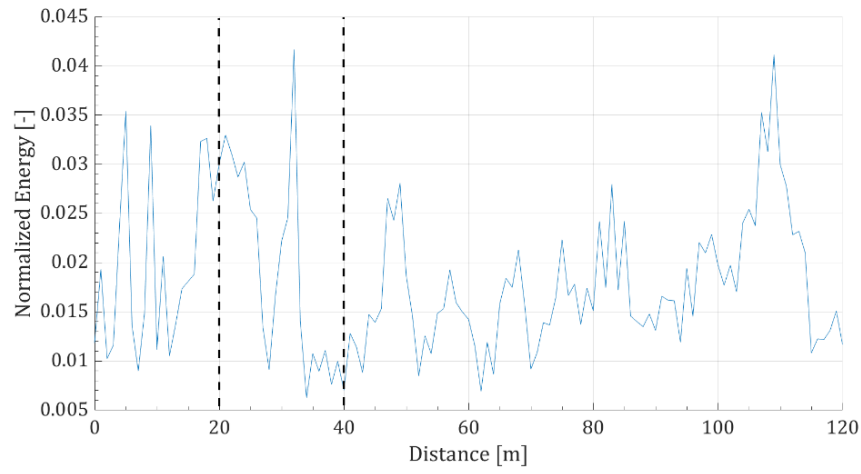
b)
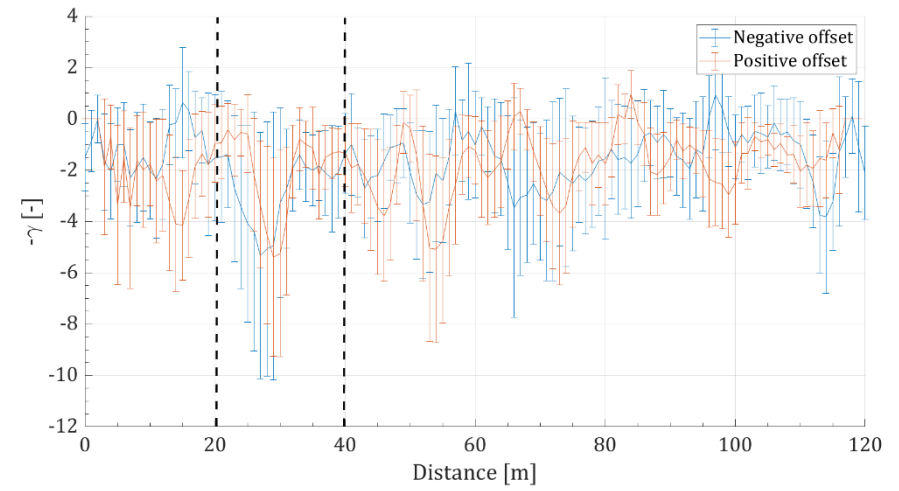
c)

d)

Figure 44. Results for a) Energy, b) Energy decay exponent, c) Attenuation coefficient, d) Autospectrum stack plots.

4.2.7.   Comparison with a 2D synthetic model

From all the 2D synthetic models developed by Colombero et al., (2019), one configuration that could be useful for the comparison of the response of the pipeline within the embankment was extracted, meaning a buried cavity surrounded by homogeneous material. The cavity has a 4 x 4 m square section and is characterized by air velocity (340 m/s). It is buried at 4 m depth, enclosed in a high velocity medium (2675 m/s). Synthetic results for all methods are presented in Figure 45.
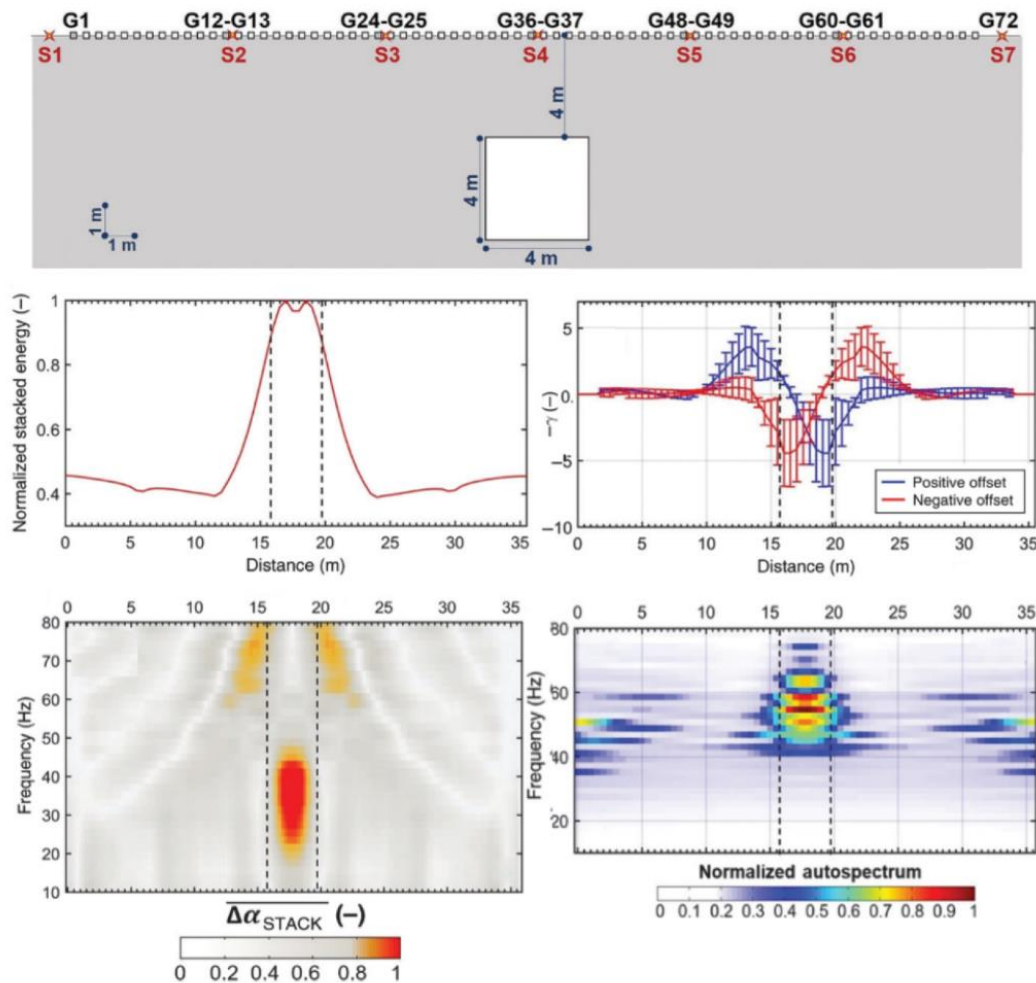

Figure 45. Results from synthetic model developed by Colombero et al., (2019). Extracted and modified from Colombero et al., (2019).

Overall, plots of energy, attenuation coefficient (stacked in absolute value) and autospectrum are showing the same response as for the 2D synthetic model developed by Colombero et al., (2019), meaning that the outstanding response depicted in the results is coming from the effect of the empty pipeline structure surrounded by a higher velocity material. As a weak difference, in the energy decay exponent, only negative values are found around the pipeline and no energy concentrations are found on the two sides of its structure.

It must be eventually noticed that the data processed in this thesis were not acquired in the open field, but on a 3D linear element that complicates wave propagation, with the presence of guided surface waves propagating along the embankment, trapped within it and likely scattering and reflecting at the external boundaries. Nevertheless, the effectiveness of the methods appears still valid. 3D numerical models of surface wave propagation should be designed in the future to fully understand the influence of the embankment shape on wave propagation and on the obtained results.

4.3.   Depth estimation

As discussed in Chapter 2, SWs are dispersive waves, and their phase velocity depends on the propagating frequency or wavelength. This dependency results in a dispersion curve, linking frequency (or wavelength) and phase velocity. The wavelength can be expressed as the ratio between phase velocity and frequency.

If one or more dispersion curves can be extracted from the landstreamer data, the frequency axis of autospectrum and attenuation coefficient plots can consequently be converted into wavelength. This representation can give a better idea of the depth of the anomalies that are visualized by the methods. Generally, the depth of the anomalies is indeed considered to be around 1/3 or ½ of the interested wavelengths (Zerwer et al., 2005). Even if this method is very rough, it provides a more representative imaging of the SW parameters computed as a function of frequency.

In this work, it was used an average dispersion curve (Figure 46a) extracted from the positive offset data in an independent study, to show the conversion of the autospectrum plot. The obtained results are shown in Figure 47.
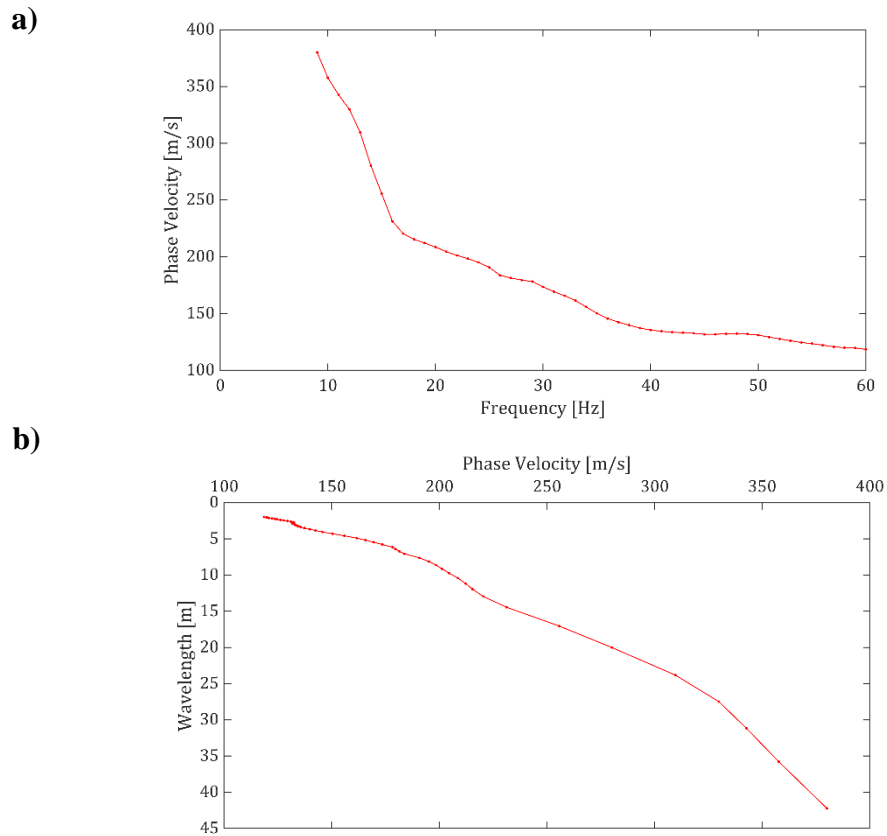
a)

b)

Figure 46. Average dispersion curve for the investigated line as a function of a) frequency and b) wavelength.

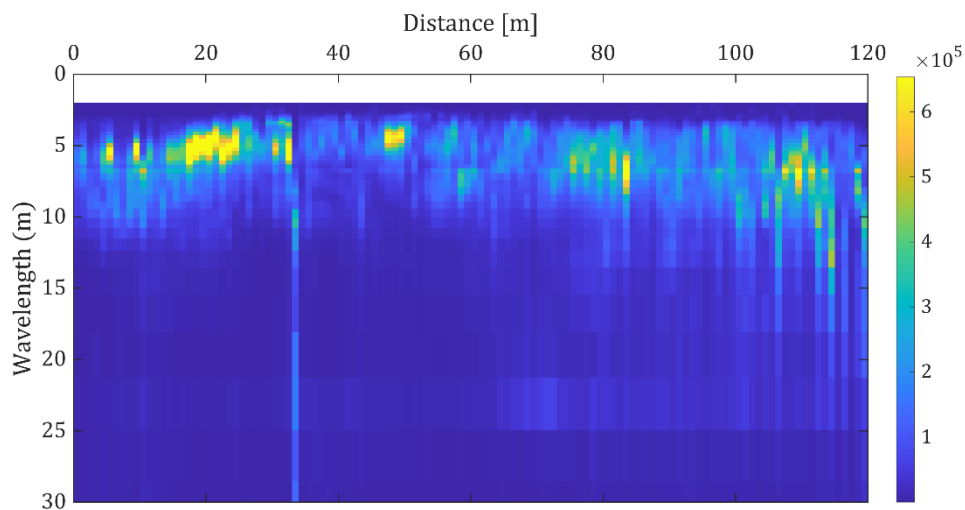*Figure 47. Autospectrum results converted as a function of wavelength using the reference dispersion curve of Figure 46.*

High energy concentrations are found in the results below 10 m of wavelength. These energy concentrations seem to follow the morphology of the low velocity layer ($V_P < 500$ m/s) depicted at the top of the velocity model retrieved from refraction tomography. In particular,

a clear deepening of this anomaly is found in the first 20 m of the line, coherent in shape with the low velocity anomaly of the refraction model.

The pipeline anomaly is highest between 4-6 m of wavelength. These wavelengths are consistent with its known embedment depth (2-4 m, i.e. approximately ½ of the wavelength).
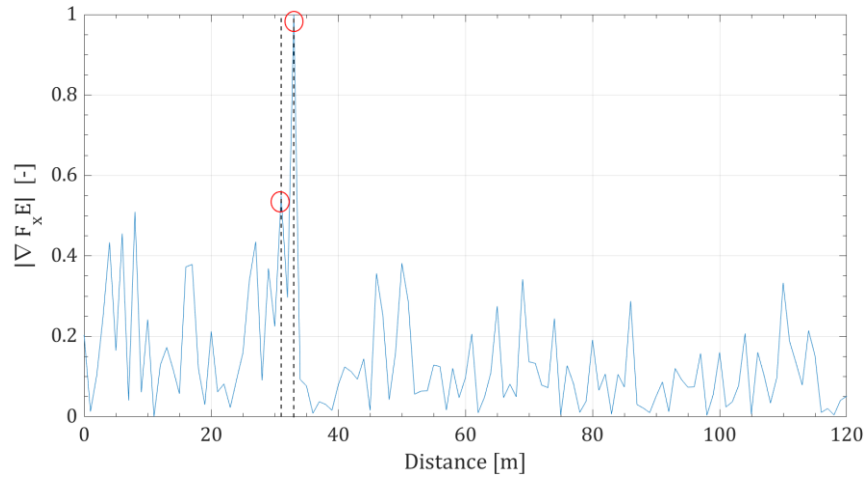
4.4. Horizontal gradient analysis

The horizontal gradient ∇F_x of all the four stacked parameters was computed to highlight the lateral variations and to improve the location of the pipeline. For energy and energy decay exponent methods, ∇F_x was computed directly on the vectors containing the values in each position of the survey line, while for attenuation coefficient and autospectrum, results were summed along the frequency axes to obtain a vector with single values at the different distances, to be compare with the other two methods. The absolute values and normalization of these vector were calculated and results for each method are presented in Figure 48.

For energy and autospectrum gradients (Figure 48a and Figure 48c), the maxima are clearly located within 20 and 40 m, while the energy decay exponent and attenuation coefficient plots (Figure 48b and Figure 48d) showed more picks along the horizontal direction.

The same criteria followed by Colombero et al., (2019) for location of sharp lateral variations was choose for the location of the pipeline: for energy and autospectrum plots, the maximum value of energy gradient corresponds with the estimated location of the pipeline (red circles in Figure 48.a and Figure 48.c). For the energy decay exponent plots, the criterium was to take the local minimum values between two gradient peaks for positive and negative offset (red circles in Figure 48.b). The dashed lines correspond with the average value of positive and negative offset gradient minima and the location of the pipeline is within. For attenuation coefficient results, a similar criterium was followed, selecting the local minimum values (red circles) between two gradient peaks as the estimated location of the pipeline (Figure 48.d).

Energy and autospectrum results showed that the location of the pipeline is between 31 and 34 m, while energy results of energy decay and attenuation coefficient showed that the estimated location is between 28 and 35 m.
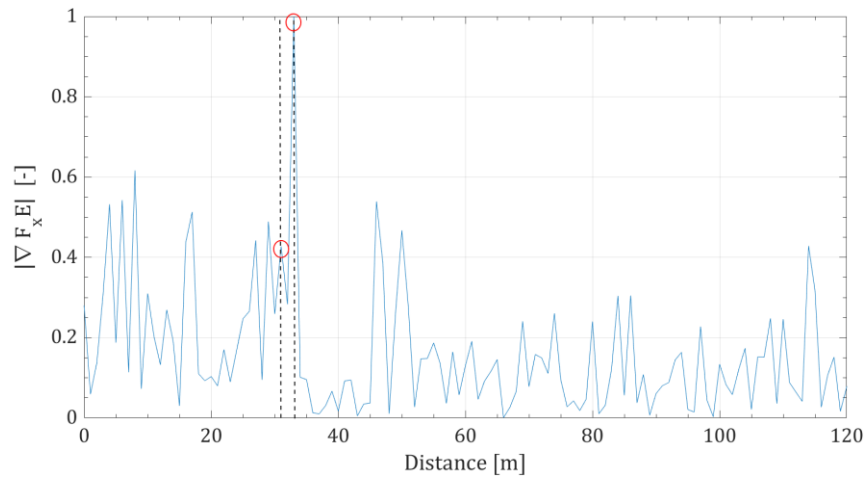
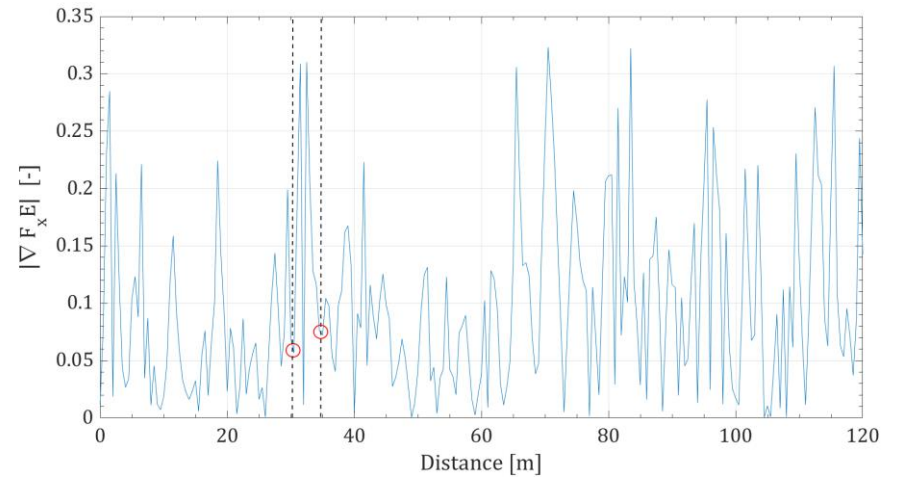**a)**

b)
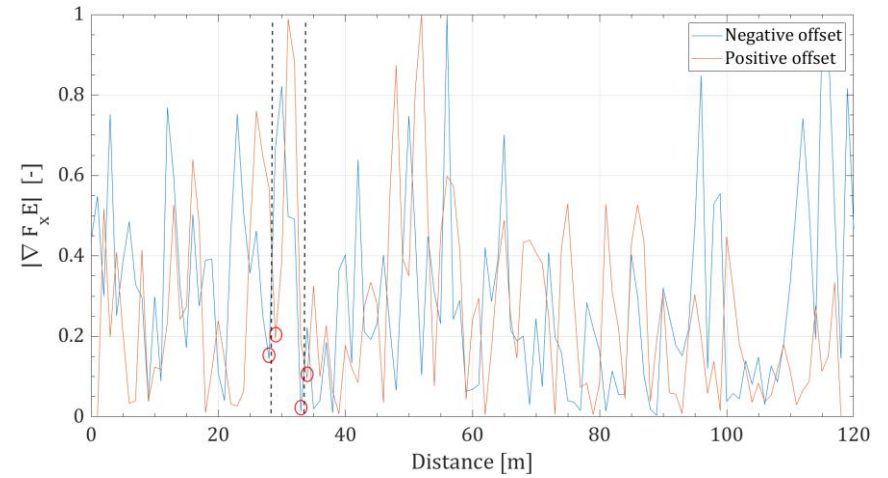
c)

d)

Figure 48. Horizontal gradient results for a) Energy, b) Energy decay exponent, c) Autospectrum, d) Attenuation coefficient.

Chapter 5

Conclusions

The overall contribution of this work is the presentation of a new method for characterization of embankments using the combination of four fast SW processing techniques. Based on the discussion of the results in Chapter 4, the major conclusions and contributions are listed as follows:

1) The seismic data set obtained in a fast way with landstreamer acquisition are proved in this work to be of good quality. The noise due to the receiver configuration is reduced. This was verified during the selection of the travel times for refraction tomography, where the noise in every CSG was not an impediment for first arrival time picking. Nevertheless, the positive offset data showed a better quality of the results.

2) Trace normalization in each CSG before the application of the four methods improves the results, as demonstrated by comparing trace-normalized and standard autospectral results for positive offset data.

3) Trace normalization in each CSG before the application of the four methods improves the results, as demonstrated by comparing trace-normalized and standard autospectral results for positive offset data.

4) Refraction tomography is time consuming and requires slow and accurate processing and inversion to generate the final velocity model. In addition, the obtained velocity model is smooth and hides the pipeline presence. As a consequence, small size targets or weaknesses within the embankment risk to be ignored in the interpretation.

5) The four SW-methods work effectively for the identification and location of the pipeline within the embankment. Beside this target, interesting anomalies likely due to geological and geotechnical contrast within the embankment material were discovered and confirmed by refraction results. Overall, positive offset plots effectively depicted the position of the pipeline. Negative offsets instead, had much more noise that could have partially affected the quality of the results. The stacked results would have benefited from data of optimal quality along both offsets.

6) All methods depict very well the response of the pipeline as high energy concentrations and strong attenuation in correspondence, as the effect of propagation from a high- to a low-velocity material.

7) Horizontal gradient computation allowed to quantitatively estimate the location of the pipeline. Results showed that the pipeline structure is located within 28 and 35 m.

8) Surface waves analysis allowed to estimate the embedment depth at 2-4 m.

9) The results provided in this work demonstrate that the combination of landstreamer acquisition and the four SW-methods analysis is a fast and efficient tool for embankments monitoring. The effectiveness of these tools was verified for the first time in this work and is presented as a novel technique for integrity of embankments assessments.

The following perspectives are proposed for future studies:

1) The automatic location of the anomalies, as the application of all the methods requires a visual analysis of the results or of their horizontal gradients.

2) The development of 3D synthetic models that simulates the complex wave propagation within embankments.

3) The organization of the acquisition phase considering a more balanced coverage along the whole embankment.

4) Tests on the applicability of the SW-methods directly on the field to visualize the results in nearly real time, since all methods are straightforward and fast after data acquisition.

References

Abdulsamad, F., Revil, A., Ahmed, A. S., Coperey, A., Karaoulis, M., Nicaise, S., & Peyras, L. (2019). Induced polarization tomography applied to the detection and the monitoring of leaks in embankments. Engineering Geology, 254(April), 89–101. https://doi.org/10.1016/j.enggeo.2019.04.001

Bergamo, P., & Socco, L. V. (2014). Detection of sharp lateral discontinuities through the analysis of surface-wave propagation. 79(4).

Boiero, D., & Socco, L. V. (2011). The meaning of surface wave dispersion curves in weakly laterally varying structures. 2007, 561–570. https://doi.org/10.3997/1873-0604.2011042

Borgatti, L., Forte, E., Mocnik, A., Zambrini, R., Cervi, F., Martinucci, D., Pellegrini, F., Pillon, S., Prizzon, A., & Zamariolo, A. (2017). Detection and characterization of animal burrows within river embankments by means of coupled remote sensing and geophysical techniques : Lessons from River Panaro (northern Italy). Engineering Geology, May, 0–1. https://doi.org/10.1016/j.enggeo.2017.06.017

Colombero, C., Comina, C., & Socco, L. V. (2019). Imaging near-surface sharp lateral variations with surface-wave methods - Part 1: Detection and location. Geophysics, 84(6), EN93–EN111. https://doi.org/10.1190/GEO2019-0149.1

Comina, C., Vagnon, F., Arato, A., Fantini, F., & Naldi, M. (2020). A new electric streamer for the characterization of river embankments. Engineering Geology, 276(May), 105770. https://doi.org/10.1016/j.enggeo.2020.105770

Di-Prinzio, M., Bittelli, M., Castellarin, A., & Rossi, P. (2010). Application of GPR to the monitoring of river embankments. Journal of Applied Geophysics, 71(2–3), 53–61. https://doi.org/10.1016/j.jappgeo.2010.04.002

Dobrin, M. B. (1960). Introduction to Geophysical Prospecting.

Everest Geophysics S.L. (2020). Everest Geophysics S.L. https://everestgeophysics.com/methods/seismic/masw/

Fazio, L. (2019). Definizione delle curve di fragilità per la diga in materiali sciolti nel comune di Arignano.

Fitts, C. R. (2013). Field Exploration and Wells, in Groundwater Science (Second Edition).

Foti, S., Hollender, F., & Garofalo, F. (2018). Guidelines for the good practice of surface wave analysis : a product of the InterPACIFIC project. https://doi.org/10.1007/s10518-017-0206-7

Geotom. (2014). Installing and running the three-dimensional tomography program: GEOTOMCG (Issue January).

Lange, A., & Schuck, G. (2007). Seismic Methods (pp. 337–402).

Liberty, L. M., & Gribler, G. (2014). Development of land streamer technologies for estimating shear wave velocities in an urban environment. 08.

Manzoni de G., S. V. (2001). SECUENCIA BÁSICA DE PROCESAMIENTO DE DATA SÍSMICA PARA OBTENER DATOS FINALES , ORIENTADA A ESTUDIANTES DE INGENÍERIA GEOFÍSICA.

Miller, G. F., & Pursey, H. (1954). The Field and Radiation Impedance of Mechanical Radiators on the Free Surface of a Semi-Infinite Isotropic Solid Article cited in : https://doi.org/10.1098/rspa.1954.0134

Miller, R., & Steeples, D. (1994). Applications of shallow high-resolution seismic reflection to various environmental problems. 31, 65–72.

Nasseri-Moghaddam, A., Cascante, G., & Hutchinson, J. (2005). A new quantitative procedure to determine the location and embedment depth of a void using surface waves. Journal of Environmental and Engineering Geophysics, 10(1), 51–64. https://doi.org/10.2113/JEEG10.1.51

Park, C. B., Miller, R. D., Xia, J., Julian, I., & Survey, K. G. (2007). Multichannel analysis of surface waves (MASW)—. SEG, Figure 1, 60–64.

Perri, M. T., Boaga, J., Bersan, S., Cassiani, G., Deiana, R., Simonini, P., & Patti, S. (2014). River embankment characterization: the joint use of geophysical and geotechnical techniques. Journal of Applied Geophysics. https://doi.org/10.1016/j.jappgeo.2014.08.012

Piemonte, E. R. (n.d.). Piemonte Parchi. http://www.piemonteparchi.it

Ramirez C., G. C. (2011). ESTUDIO GEOELÉCTRICO CON FINES DE PROSPECCIÓN DE AGUAS SUBTERRÁNEAS EN ZONAS ALEDAÑAS A LA ESTACIÓN TERRENA DE CONTROL DEL SATÉLITE SIMÓN BOLÍVAR, ESTADO GUÁRICO.

Sheriff, R. E., & Geldart, L. P. (1995). Exploration Seismology (Second). Cambridge University Press.

Telford, W. ., Geldart, L. ., & Sheriff, R. . E. (1990). Applied geophysics. In Nature (2 nd, Issue 3212). https://doi.org/10.1038/127783a0

Van der Veen, M., Spitzer, R., Green, A. G., & Wild, P. (2001). Design and application of a towed land-streamer system for cost-effective 2-D and pseudo – 3-D shallow seismic data acquisition. 66(2), 482–500.

Veen, Michiel Van Der, & Green, A. G. (1998). Land streamer for shallow seismic data acquisition : Evaluation of gimbal-mounted geophones. 63(4), 1408–1413.

Xia, J., Miller, R. D., Park, C. B., & Tian, G. (2002). Determining Q of near-surface materials from Rayleigh waves. 51, 121–129.

Zerwer, A., Polak, M. A., & Santamarina, J. C. (2005). Detection of surface breaking cracks in concrete members using Rayleigh waves. Journal of Environmental and Engineering Geophysics, 10(3), 295–306. https://doi.org/10.2113/JEEG10.3.295